

UNCERTAINTY QUANTIFICATION OF SYNCHROSQUEEZING TRANSFORM UNDER COMPLICATED NONSTATIONARY NOISE

HAU-TIENG WU AND ZHOU ZHOU

ABSTRACT. We propose a bootstrapping algorithm to quantify the uncertainty of the time-frequency representation (TFR) generated by the short-time Fourier transform (STFT)-based synchrosqueezing transform (SST) when the input signal is oscillatory with time-varying amplitude and frequency and contaminated by complex nonstationary noise. To this end, we leverage a recently developed high-dimensional Gaussian approximation technique to establish a sequential Gaussian approximation for nonstationary random processes under mild assumptions. This result is of independent interest and enables us to quantify the approximate Gaussianity of the random field over the time-frequency domain induced by the STFT. Building on this foundation, we establish the robustness of SST-based signal decomposition in the presence of nonstationary noise. Furthermore, under the assumption that the noise is locally stationary, we develop a Gaussian auto-regressive bootstrap framework for uncertainty quantification of the TFR obtained via SST and provide a theoretical justification. We validate the proposed method through simulated examples and demonstrate its utility by analyzing spindle activity in electroencephalogram recordings.

Keywords: Sequential Gaussian Approximation; nonstationary noise; bootstrap; short-time Fourier transform; synchrosqueezing transform

1. INTRODUCTION

Uncertainty quantification is crucial for applying time-frequency analysis [12] tools, particularly the synchrosqueezing transform (SST) [8], to study nonstationary time series, as it ensures the reliability and interpretability of the extracted features. In real-world applications, such as biomedical signal processing, climate modeling, and finance, time series data are often contaminated by nonstationary noise and influenced by various external factors. Without properly quantifying uncertainty, the interpretation of the resulting time-frequency representations (TFR), which is a function defined on the time-frequency (TF) domain, might be misleading, leading to incorrect conclusions about the underlying dynamics. By incorporating uncertainty quantification, we can more reliably differentiate true oscillatory patterns from artifacts, improve the robustness of feature extraction, and guide decision-making in practical applications. Furthermore, rigorous uncertainty estimation provides a foundation for statistical inference, enabling hypothesis testing and model validation in TF analysis. In this paper, we focus on establishing the uncertainty quantification of SST under complicated nonstationary noise.

The first mathematical challenge in this direction is to characterize the distribution of the TFR determined by the short-time Fourier transform (STFT) [12],

which serves as the foundation for the SST, when the input is a non-Gaussian and nonstationary random process with a nontrivial dependence structure. In many existing studies, particularly those focused on SST [27, 3, 35, 25], this step is often bypassed by modeling the signal as a continuous function and the noise as a tempered distributed stationary Gaussian random process Φ . Under this continuous framework, when the window function h is chosen to be a Schwartz function, the STFT, defined as $V_\Phi(t, \eta) := \Phi(h(\cdot - t)e^{i2\pi\eta(\cdot - t)})$, where $t \in \mathbb{R}$ is time and $\eta \in \mathbb{R}$ is frequency, is automatically a complex Gaussian random field. This setting allows researchers to concentrate on the algorithm's nonlinearity. However, this assumption is often unrealistic in practice, as the input data are typically discrete and noise is usually non-Gaussian and nonstationary. Under a discrete framework, the distribution of the TFR determined by the discrete STFT remains largely unexplored, with the exception of recent efforts [36] examining finite collections of time-frequency pairs. Intuitively, since the numerical implementation involves a weighted summation of random variables, the resulting distribution should approximate a Gaussian random field when the window length is sufficient to encompass many samples and the noise satisfies mild dependence and moment conditions, by the central limit theorem. Although numerical evidence supports this intuition, the precise conditions under which the numerically implemented TFR closely approximates a Gaussian random field, particularly when the input noise is non-Gaussian and nonstationary, are not yet fully understood. In this paper, we apply a recently developed *high-dimensional Gaussian approximation* technique to establish a *high-dimensional sequential Gaussian approximation* suitable for analyzing the discrete STFT. We show that, under appropriate discretization and mild conditions on the noise, the numerically computed TFR via discrete STFT is asymptotically close to a complex Gaussian random field. This result extends the existing literature by rigorously addressing the statistical properties of the discrete STFT under more general and practically relevant noise settings.

The second challenge in developing a bootstrapping algorithm is determining how accurately we can recover the underlying signal, and hence the noise, so that the noise can be effectively resampled. We focus on oscillatory signals that can be well modeled by the adaptive harmonic model (AHM) [8], where the signal exhibits oscillations with slowly varying amplitude and frequency. To recover the underlying signal, we adopt the reconstruction formula based on the SST, motivated by empirical observations suggesting that SST exhibits strong robustness to various forms of nonstationary noise. To date, the robustness of this SST-based reconstruction has been theoretically established under noise models involving distributed stationary random processes [27] and distributed nonstationary random processes with stationary correlation structures [3]. However, real-world noise is often non-Gaussian and fully nonstationary, and theoretical guarantees in this setting have been lacking. In this paper, we establish the robustness of the SST-based reconstruction formula for signals satisfying the AHM, even when the signal is contaminated by fully nonstationary noise.

The third challenge is designing a bootstrapping method to quantify the uncertainty of the TFR determined by SST. In practice, we often lack detailed information about the noise structure, including its stationarity. To address this, we assume the noise is locally stationary and apply the recently developed time-varying autoregressive (tvAR) approximation [10] to obtain a reasonable model of the noise.

This approximation enables us to resample the noise. However, a key difficulty lies in understanding how the approximation error propagates through the nonlinear operations involved in SST during the bootstrapping process. We show that the TFR of a locally stationary noise process determined by SST can be accurately approximated through bootstrapping based on the tvAR approximation, thereby enabling the desired uncertainty quantification.

The contributions of this paper are threefold. First, we establish that when a nonstationary time series is generated by a filtration mechanism and satisfies mild moment and temporal dependence conditions, the TFR determined by the discrete STFT can be well approximated by a Gaussian random field in the time-frequency domain (see Theorem 3.2). To achieve this, we apply a recently developed high-dimensional Gaussian approximation technique [17] together with a blocking strategy [6] to construct a sequential high-dimensional Gaussian approximation. This result is of independent interest and enables a rigorous quantification of the Gaussianity of the TFR determined by the discrete STFT. Second, we investigate the robustness of the SST-based reconstruction formula when the input signal is an oscillatory signal satisfying the AHM and is corrupted by a nonstationary time series generated by the same filtration mechanism (see Theorem 4.2). A critical aspect of this analysis is understanding the interplay between the continuous and discrete formulations of the STFT, and consequently of the SST. In particular, we study how the discrete STFT approximates its continuous counterpart and how the discretization of SST connects the TF analysis in the discrete and continuous frameworks. Third, building on these findings, and under the additional assumption that the noise is locally stationary, we develop a tvAR-approximation-based bootstrapping algorithm for the TFR determined by SST, enabling rigorous uncertainty quantification (see Theorem 5.1).

Notation: For a random vector $v \in \mathbb{R}^d$, denote $|v|$ to be its Euclidean norm and $|v|_\infty$ to be its ℓ^∞ norm. For a random variable X , denote $\|X\|_q$ to be its \mathcal{L}^q norm. For two sequences a_n and b_n , denote $a_n = O_{\ell^2}(b_n)$ to state that a_n/b_n is bounded in \mathcal{L}^2 norm. Similarly, $a_n = o_{\ell^2}(b_n)$ says that a_n/b_n converges to 0 in \mathcal{L}^2 norm.

2. ALGORITHM AND MATHEMATICAL BACKGROUND

2.1. discrete short-time Fourier transform (STFT). Take a time series $\{X_l\}_{l \in \mathbb{Z}}$. The *discrete STFT* of $\{X_l\}_{l \in \mathbb{Z}}$ associated with a unit vector $\mathbf{h} \in \mathbb{R}^{2m+1}$, where $m \in \mathbb{N}$, as the window, is defined as

$$(1) \quad \mathbf{V}_X^{(\mathbf{h})}(l, \eta) := \sum_{j=l-m}^{l+m} X_j \mathbf{h}(j-l) e^{-i2\pi\eta(j-l)},$$

where $l \in \mathbb{Z}$ and $\eta \in [0, 1/2)$ is the frequency to explore. Here, m is the length of truncation related to the kernel bandwidth and is chosen by the user.

2.2. Continuous STFT and its discretization. We shall mention that the discrete STFT (1) is directly related to the discretized version of the *continuous STFT*. Recall the continuous STFT:

$$(2) \quad V_f^{(\mathbf{h})}(t, \xi) := \int_{-\infty}^{\infty} f(x) \mathbf{h}(x-t) e^{-i2\pi\xi(x-t)} dx,$$

where f is a continuous tempered distribution and \mathbf{h} is a symmetric Schwartz function with unit L^2 norm and supported on $[-\beta, \beta]$, where $\beta > 0$ is chosen by the

user to control the spectral resolution. A more general setup is certainly possible; however, it does not provide additional insight into the main focus of this paper. Therefore, we adopt this specific setup for the purposes of this study. In general, when the sampling rate is q Hz and we have n sampling points over the period $[0, n/q]$, (2) is discretized by the Riemann sum as

$$(3) \quad V_f^{(\mathbf{h})}(t_l, \eta) \approx \frac{1}{q} \sum_{j=1}^n f(t_j) \mathbf{h}(t_j - t_l) e^{-i2\pi\eta(t_j - t_l)},$$

where $f(t_j)$ is set to 0 when $t_j < 0$ or $t_j > n/q$ (that is, pad the signal by 0, $t_l = l/q$, $l = 1, \dots, n$, and $\eta \in [0, q/2)$ is the frequency of interest. We call the right hand side of (3) the *discretized STFT*. This discretization approximation \approx holds when q is sufficiently large, which we assume from now. We will precisely quantify it below for our analysis purpose. Set $\mathbf{h} \in \mathbb{R}^{2\lceil\beta q\rceil+1}$

$$(4) \quad \mathbf{h}(k) = \frac{1}{\sqrt{q}} \mathbf{h} \left(-\beta + \frac{k-1}{q} \right), \quad k = 1, \dots, 2\lceil\beta q\rceil + 1,$$

where the normalization $\frac{1}{\sqrt{q}}$ guarantees that $\|\mathbf{h}\|$ is of order 1 when q is large, since $\sum_{k=1}^{2\lceil\beta q\rceil} \mathbf{h}(k)^2 \rightarrow \int_{-\beta}^{\beta} |\mathbf{h}(t)|^2 dt = 1$, when $q \rightarrow \infty$. In other words, we discretize the window \mathbf{h} by $2\lceil\beta q\rceil + 1$ points. In this setup, we connect the discretized STFT and the discrete STFT (1) with a normalization factor $1/\sqrt{q}$; that is, if we set $X_j = f(t_j)$, we obtain

$$(5) \quad V_f^{(\mathbf{h})}(t_l, \eta) \approx \frac{1}{\sqrt{q}} \sum_{j=l-\lceil\beta q\rceil}^{l+\lceil\beta q\rceil} X_j \mathbf{h}(j-l) e^{-i2\pi\eta(t_j - t_l)} =: V_X^{(\mathbf{h})}(t_l, \eta) = \frac{1}{\sqrt{q}} \mathbf{V}_X^{(\mathbf{h})}(l, \eta).$$

2.3. Synchrosqueezing transform (SST). SST is derived from the continuous STFT, and numerically implemented via a direct discretization. Following the same notation in Section 2.2. Recall that the *STFT-based SST* of f with *resolution* $\alpha > 0$ is defined as

$$(6) \quad S_f^{(\mathbf{h})}(t, \xi) := \int_0^\infty V_f^{(\mathbf{h})}(t, \eta) g_\alpha(\xi - O_f^{(\nu)}(t, \eta)) d\eta,$$

where $\xi > 0$ is the positive frequency we have interest and $O_f^{(\nu)}(t, \eta)$ is the *reassignment rule* defined by

$$(7) \quad O_f^{(\nu)}(t, \eta) := \begin{cases} \frac{-1}{2\pi i} \frac{V_f^{(\mathbf{h}')} (t, \eta)}{V_f^{(\mathbf{h})} (t, \eta)} + \eta & \text{if } |V_f^{(\mathbf{h})}(t, \eta)| > \nu \\ -\infty & \text{otherwise,} \end{cases}$$

where $\nu \geq 0$ is the chosen threshold, $g_\alpha : \mathbb{C} \rightarrow \mathbb{R}$ approximates the δ measure with the support at $\{0\}$ when $\alpha \rightarrow 0$. The parameter α dictates SST's resolution in the frequency-axis. For clarity, below we adopt $g_\alpha(z) = \frac{1}{\sqrt{\pi\alpha}} e^{-|z|^2/\alpha}$, which has the L^1 norm 1. The nonlinearity of SST as a transform stems from the reliance of equation (6) on the reassignment rule. This rule offers insights into the signal's instantaneous frequency [8, 28]. The main advantage of SST over the STFT lies in its ability to enhance the contrast of the TFR by using the phase information in the STFT via (7), and hence mitigate the effects of the uncertainty principle, provided that the input signal satisfies certain oscillatory conditions like the AHM. This

improvement facilitates the detection of oscillatory components and enables more accurate estimation of key quantities such as the instantaneous frequency. As a result, SST supports more effective denoising and amplitude modulation estimation through its reconstruction formula.

Numerically, when the sampling rate is q Hz and we have n sampling points sampled at i/q , where $i = 1, \dots, n$, over the period $[0, n/q]$, STFT-based SST is implemented by a direct discretization. Define $\mathbf{h} \in \mathbb{R}^{2\lceil\beta q\rceil+1}$ as (4) and $\mathbf{Dh} \in \mathbb{R}^{2\lceil\beta q\rceil+1}$ so that

$$(8) \quad \mathbf{Dh}(k) = \frac{1}{\sqrt{q}} \mathbf{h}' \left(-\beta + \frac{k-1}{q} \right), \quad k = 1, \dots, 2\lceil\beta q\rceil + 1.$$

Denote $V_X^{(\mathbf{Dh})}(t_l, \eta_k)$ to be the discretization of the continuous STFT of f with the window \mathbf{h} replaced by \mathbf{h}' . The STFT-based SST with threshold $\nu \geq 0$ is thus numerically implemented by the Riemann sum

$$(9) \quad S_X^{(\mathbf{h})}(t_l, \xi_j) := \frac{C}{d} \sum_{k=1}^d V_X^{(\mathbf{h})}(t_l, \eta_k) g_\alpha(\xi_j - O_X^{(\nu)}(t_l, \eta_k)),$$

where $d \in \mathbb{N}$ means d uniform points on $[0, C]$ in the frequency axis, $0 < C \leq \frac{q}{2}$ indicates the chosen spectral range of interest, $\xi_j \in [0, q/2)$ is the positive frequency we have interest and $O_X(t_l, \eta_k)$ is the *reassignment rule* defined by

$$(10) \quad O_X^{(\nu)}(t_l, \eta_k) := \begin{cases} \frac{-1}{2\pi i} \frac{V_X^{(\mathbf{Dh})}(t_l, \eta_k)}{V_X^{(\mathbf{h})}(t_l, \eta_k)} + \eta_k & \text{if } |V_X^{(\mathbf{h})}(t_l, \eta_k)| > \nu \\ -\infty & \text{otherwise.} \end{cases}$$

In practice, while C can be chosen as large as \sqrt{q} , particularly when no background information is available, it is typically set to a sufficiently large constant to capture enough spectral information, depending on the application. The parameter ν is usually selected as a small multiple of the variance of the input signal to enhance algorithmic stability. For example, ν is often set to 10^{-6} .

Remark. We comment that the selection of ξ_l in practical implementations holds significance. Following the classical Nyquist-Shannon sampling theory, a natural inclination based on the selected window \mathbf{h} and discretization would be to opt for $\xi_l = \frac{l}{2\beta}$, where $l = 1, \dots, \lceil\beta q\rceil$. On the other hand, studies in discrete Fourier transform have shown that adopting a finer grid can effectively counter spectral leakage issues [13]. In practice, we find that a finer grid in SST provides benefit, while the optimal grid choice, and its interaction with α , has not been explored systematically. Combined the above facts, an alternative choice of ξ_i , such as $\xi_l = l/(2\beta q)$ with $l = 1, \dots, \lceil\beta q^{3/2}\rceil$, might offer not only practical but also theoretical benefits. A thorough investigation of this issue lies beyond the scope of this paper and will be pursued in future work.

2.4. Mathematical model. Take a real time series $Y = \{Y_i\}_{i=1}^n$ that follows the model

$$(11) \quad Y_i = f_i + \sigma \epsilon_i,$$

where f_i is a deterministic sequence, $\sigma > 0$ might depend on n , and ϵ_i is a random process modeling noise. We detail f and ϵ term by term below.

2.5. Adaptive harmonic model. Consider an oscillatory function

$$(12) \quad f(t) = A(t) \cos(2\pi\phi(t))$$

where $\phi(t) \in C^2(\mathbb{R})$ is a monotonically increasing sequence such that $\phi'(t) > 0$, which is called *instantaneous frequency* (IF) modeling how fast the signal oscillates at time t , $A(t) \in C^1(\mathbb{R})$ is a positive function, which is called *amplitude modulation* (AM) modeling the oscillatory strength at time t . In practice, $\phi(t)$ is called the *phase* of the oscillatory signal $f(t)$. We need the following *slowly varying* assumption:

Assumption 2.1. For a nonnegative small $\varepsilon < 1$, we assume

- $\Xi_s < \phi'(t) < \Xi$ for all $t \in \mathbb{R}$, where $\varepsilon^{1/3} < \Xi_s < \Xi$ are constants;
- $|A'(t)| \leq \varepsilon A(t)$ for all $t \in \mathbb{R}$; $\Xi_a \leq A(t) \leq \Xi_A$ for all $t \in \mathbb{R}$, where $\varepsilon^{1/3} < \Xi_a < \Xi_A$ are constants.
- $|\phi''(t)| \leq \varepsilon \phi'(t)$ for all $t \in \mathbb{R}$ and $\sup_t |\phi''(t)| < M$ for some $M \geq 0$.

We refer to the deterministic function $f(t) = A(t) \cos(2\pi\phi(t))$ fulfilling Assumption (2.1) as an intrinsic mode type (IMT) function, and call this model *the adaptive harmonic model* (AHM). This model's identifiability has been established in [3]. In the traditional time series literature, it is commonly assumed that $\phi(t)$ is linear and $A(t)$ is constant; that is, $\varepsilon = 0$, so that the oscillatory signal is purely harmonic. However, in many practical applications, signals oscillate with time-varying speed and amplitude, making the harmonic model inadequate. While more complex models can be considered to better model practical signals, such as those involving multiple IMT functions or non-sinusoidal oscillations, they do not contribute additional insight for the uncertainty quantification focus of this work. Thus, for our purposes, this AHM suffices.

We sample $f(t)$ at time points $t_i := i/\sqrt{n}$ to model the discrete sequence f_i ; that is,

$$(13) \quad f_i = f(i/\sqrt{n}),$$

where $i = 1, \dots, n$. This corresponds to sampling f over the interval $[0, \sqrt{n}]$ with a uniform sampling period of $1/\sqrt{n}$. In the frequency domain, this setup implies a Nyquist rate of \sqrt{n} and a corresponding frequency resolution (or canonical frequency bin width) of $1/\sqrt{n}$.

Remark. In contrast to previous SST-related work, e.g., [8, 32, 3], in Assumption 2.1 we introduce additional uniform lower and upper bounds on $\phi'(t)$ and $A(t)$ over \mathbb{R} . These conditions do not meaningfully restrict the model of interest; rather, they are adopted to simplify the exploration and simplify the derivation of our theorems that are uniform in nature. It is important to note that both the IF and AM are permitted to grow at the rate of order $\varepsilon\sqrt{n}$ as $n \rightarrow \infty$, so the upper bound constraints are essential for establishing the desired uniform error bounds unless alternative bounding conditions are imposed. The lower bounds on frequency and amplitude serve to prevent degeneracy. Particularly, the subscript s in Ξ_s suggests “separation”, which controls spectral leakage. When analyzing multiple components is of interest, the analysis is a straightforward generalization with assumption that IF of different components are separated by Ξ_s . Moreover, we modify the control of A' , replacing the condition $|A'(t)| \leq \varepsilon\phi'(t)$ with $|A'(t)| \leq \varepsilon A(t)$. This adjustment is made to highlight the role of the amplitude more clearly in the final theoretical results.

2.6. High dimensional non-stationary (HDNS) model and non-stationary noise (NSN) model. Next, $\{\epsilon_i\}_{i=1}^n$ is a centered non-stationary noise process whose data generating mechanism may evolve both smoothly and abruptly over time. To put structures on ϵ_i , we first consider the following filtration-based high dimensional non-stationary (HDNS) time series

$$(14) \quad z_i = (z_{i,1}, \dots, z_{i,d}) := \mathcal{G}_i(\mathcal{F}_i) \in \mathbb{R}^d$$

for $i = 1, \dots, n$, where $d \in \mathbb{N}$, $\mathcal{G}_i = (\mathcal{G}_{i,1}, \dots, \mathcal{G}_{i,d}) : \mathbb{R}^\infty \rightarrow \mathbb{R}^d$ is a measurable function, $\mathcal{F}_i := (\dots, e_{i-1}, e_i)$ is a sequence of i.i.d. random variables $\{e_i\}$, \mathcal{G}_i is the causal filtration mechanism at time i that takes a sequence of i.i.d. random variables and outputs a d -dimensional random vector. When $d = 1$, we simply say the time series satisfies the non-stationary noise (NSN) model.

To quantify the dependence structure of z_i , consider an i.i.d. copy of $\{e_i\}$, denoted as $\{\hat{e}_i\}$, and define $\mathcal{F}_{i,i-k} := (\dots, e_{i-k-1}, \hat{e}_{i-k}, e_{i-k+1}, \dots, e_i)$. The temporal dependence structure is quantified by the entrywise uniform functional dependence measure:

$$(15) \quad \theta_{q,j}(k) := \sup_{1 \leq i \leq n} (\mathbb{E}[|\mathcal{G}_{i,j}(\mathcal{F}_i) - \mathcal{G}_{i,j}(\mathcal{F}_{i,i-k})|^q])^{1/q},$$

and the uniform functional dependence measure

$$(16) \quad \theta_q(k) := \max_{1 \leq j \leq d} \theta_{q,j}(k),$$

which quantify how the k -step historical input impacts the current output, and the quantification is uniform over the whole time series. We shall mention that the quantity $\theta_q(k)$ here depends on the maximum of all entries, which is different from the L^r norm-based physical dependence measure, where $r \geq 2$, considered in [21, Equation (3)]. The cumulative tail dependence is needed to control the auto-covariance structure of the time series, and it is quantified by

$$(17) \quad \Theta_q(k) := \max_{1 \leq j \leq d} \sum_{l=k}^{\infty} \theta_{q,j}(l).$$

The noise ϵ_i is then modeled as (14) with $d = 1$. Note that in general z_i is not a martingale.

Example. The piecewise locally stationary (PLS) with r break points (PLS(r)) [37] is a special case of the HDNS model. We say $\{\epsilon_i\}_{i=1}^n$ satisfies PLS(r) if there exist constants $0 = s_0 < s_1 < \dots < s_r < s_{r+1} = 1$ and $r + 1$ measurable functions $\mathcal{G}_0, \dots, \mathcal{G}_r$ as nonlinear causal filters such that

$$(18) \quad \epsilon_i = \mathcal{G}_j(t_i, \mathcal{F}_i), \quad \text{if } s_j < t_i \leq s_{j+1},$$

$j = 0, 1, \dots, r$, where $t_i = i/n$, and the time series is locally stationary [7] between s_j and s_{j+1} in the sense that the data generation mechanism changes slowly. This model says that the data generation mechanism changes abruptly at s_j , $j = 1, 2, \dots, r$, due to the change of filtering mechanism from \mathcal{G}_{j-1} to \mathcal{G}_j . Note that a PLS(r) model allows abrupt changes in the data generation mechanism, which allows us to better model the nonstationary noise and artifact we encounter in real-world. When $r = 0$, that is, the PLS random process is reduced to the locally stationary model [7]. We refer to [37, 38] for more discussions and examples of PLS processes and the associated dependence measures.

We need the following assumptions for (14) regarding the distribution behavior of z_i and the physical dependence structure.

Assumption 2.2. Assume that for some $p > 2$,

$$(19) \quad \theta_p(k) = O((k+1)^{-(\chi+1)}(\log(k+1))^{-A})$$

for some constants $\chi > 1$ and $A > 0$ and

$$(20) \quad \sup_{i \geq 0} \max_{1 \leq j \leq d} \mathbb{E}[|z_{i,j}|^p] < B$$

for some constant $B > 0$; that is, z_i fulfill the uniform finite p -th moment assumption for some $p > 2$ and the dependence measure $\theta_p(k)$ decays polynomially.

Note that when z_i has a finite exponential moment uniformly; that is, $\sup_{1 \leq j \leq d} \mathbb{E}[\exp(|z_{i,j}|)] < \infty$, or when the physical dependence decays exponentially; that is, $\theta_p(k) = O(\exp(-C(k+1)))$ for some constants $C > 0$, we can obtain better bounds in the upcoming theorem. Since the proof technique is similar, we focus on the above assumption to simplify the discussion.

3. GAUSSIAN APPROXIMATION OF DISCRETE STFT OF GENERAL NONSTATIONARY NOISE

To our knowledge, the distribution of discrete STFT of a locally stationary random process has been studied [36] when we consider a fixed number of time-frequency pairs. However, when the input is a more general nonstationary time series, like the nonstationary random process satisfying the NSN model, or when the number of time-frequency pairs is growing as $n \rightarrow \infty$, it is still an open problem. In this section, we extend the results of [36] to the NSN model with diverging number of time-frequency points. The main technical tool we rely on is the recently developed high-dimensional Gaussian approximation [17] for HDNS time series that generalizes earlier results from [21].

First, we extend the sequential Gaussian approximation to the HDNS model improving the results in [21, Theorem 2.2]. The proof is postponed to Section A.1.

Theorem 3.1. Suppose the HDNS time series $\{z_i\}_{i=1}^n$ satisfy Assumption 2.2 with $A > \sqrt{\chi} + 1$. Further, assume that $\|z_i\|_p \leq B_d$ for some $B_d > 0$. On a sufficiently rich probability space, there exist $\{\hat{z}_i\}_{i=1}^n$ so that $\hat{z}_i \stackrel{\mathcal{D}}{=} z_i$, and Gaussian random vectors y_i such that $y_i \sim \mathcal{N}(0, \text{cov}(z_i))$, such that

$$(21) \quad \left\| \max_{k=1, \dots, n} \left| \frac{1}{\sqrt{n}} \sum_{j=1}^k (\hat{z}_j - y_j) \right| \right\|_2 = O \left(\left(\frac{d^{\frac{3}{4} - \frac{1}{2s} - \frac{1}{p}}}{n^{\frac{1}{4} - \frac{1}{2p} - \frac{1}{2s} + \frac{1}{ps}}} \right)^{1 - \frac{1}{s} - \frac{1}{p}} \log(n)^2 \right),$$

where the implied constant depends on p and the dependence structure and moment control of z_i .

This result generalizes [21, Theorem 3.1], offering an improved convergence rate. When z_i has i.i.d. entries, d is large, and $p, s \rightarrow \infty$, the bound simplifies to $d^{3/4}n^{-1/4}$, up to a logarithmic factor. This suggests that the bound asymptotically converges to 0 when $d \asymp n^{1/3-\gamma}$ for any small γ . On the other hand, for time series with sufficiently short memory and light tail, the approximation bound established in [21] asymptotically vanishes for d as large as $O(n^{1/4-\gamma})$ for any small γ and their bound converges at the rate $n^{-1/6}$ (within a logarithm factor) as the sample size

increases. While it is possible that this bound could be further improved using alternative techniques, we find it sufficient for our current application and leave the investigation of sharper rates to future work.

To obtain a Gaussian approximation for the discrete STFT, we require the following lemma. When analyzing a nonstationary time series that satisfies the NSN model using discrete STFT, we first transform it into a HDNS time series with $d > 1$. This lemma ensures that the transformed time series continues to satisfy the same moment and dependence conditions as the original one. The proof is deferred to Section A.2.

Lemma 3.1. Suppose $\{\epsilon_i\}_{i=1}^n$ satisfies the NSN model and Assumption 2.2, with the condition $A > \sqrt{\chi} + 1$ fulfilled. Suppose $d = d(n)$ that diverges when $n \rightarrow \infty$ and consider $0 < \eta_1 < \dots < \eta_d$. Define a high dimensional time series

$$\mathbf{X}_j := [\epsilon_j \cos(2\pi\eta_1 j), \dots, \epsilon_j \cos(2\pi\eta_d j), \epsilon_j \sin(2\pi\eta_1 j), \dots, \epsilon_j \sin(2\pi\eta_d j)]^\top \in \mathbb{R}^{2d},$$

where $j = 1, \dots, n$. Then, the time series \mathbf{X}_j is HDNS satisfying Assumption 2.2, with the condition $A > \sqrt{\chi} + 1$ fulfilled.

With the above preparation, we are ready to state our main theorem about the approximate Gaussianity of discrete STFT if the input is a non-Gaussian and non-stationary random process. The proof is postponed to Section A.3.

Theorem 3.2. Suppose $\{\epsilon_i\}_{i=1}^n$ satisfies the NSN model and Assumption 2.2, with the condition $A > \sqrt{\chi} + 1$ fulfilled. Suppose $d = d(n)$ that diverges when $n \rightarrow \infty$ and consider $0 < \eta_1 < \dots < \eta_d$. Denote a complex random vector associated with the discrete STFT (1):

$$\mathbf{V}_l := [\mathbf{V}_\epsilon^{(\mathbf{h})}(l, \eta_1), \dots, \mathbf{V}_\epsilon^{(\mathbf{h})}(l, \eta_d), \mathbf{V}_\epsilon^{(\mathbf{Dh})}(l, \eta_1), \dots, \mathbf{V}_\epsilon^{(\mathbf{Dh})}(l, \eta_d)]^\top \in \mathbb{C}^{2d}$$

where \mathbf{h} and \mathbf{Dh} are defined in (4) and (8) with $m := \lceil \beta q \rceil$. Suppose $\{\hat{\epsilon}_i\}_{i=1}^n$ is a Gaussian process defined on a potentially different probability space that shares the same covariance structure of $\{\epsilon_i\}_{i=1}^n$ and denote $\hat{\mathbf{V}}_l$ to be the associated discrete STFT coefficients. We have

$$\mathbb{E} \left(\max_l \left| \frac{1}{\sqrt{n}} (\mathbf{V}_l - \hat{\mathbf{V}}_l) \right|^2 \right) \leq C' \left(\frac{d^{\frac{3}{4} - \frac{1}{2s} - \frac{1}{p}}}{n^{\frac{1}{4} - \frac{1}{2p} - \frac{1}{2s} + \frac{1}{ps}}} \right)^{\frac{2}{1 - \frac{1}{s} - \frac{1}{p}}} \log(n)^4 m^{-2},$$

where C' is a constant depending on \mathbf{h} and the moment and dependence structures of ϵ_i .

When $p, s \rightarrow \infty$, the bound becomes $d^{3/2} n^{-1/2} m^{-2}$ up to a logarithmic factor. Thus, depending on the window size m , the number of frequencies we can control is up to the order of $n^{1/3} m^{4/3}$ up to a logarithmic factor. Also, note that by construction, the variance of each entry of $\hat{\mathbf{V}}_l$ is of order 1, and the quantity $\frac{d^{\frac{3}{4} - \frac{1}{2s} - \frac{1}{p}}}{n^{\frac{1}{4} - \frac{1}{2p} - \frac{1}{2s} + \frac{1}{ps}}}$ decays polynomially to zero. We conclude that when $m \asymp n^{1/2}$,

$$\mathbb{E} \left(\max_l \left| \mathbf{V}_l - \hat{\mathbf{V}}_l \right| \right) \leq C' \left(\frac{d^{\frac{3}{4} - \frac{1}{2s} - \frac{1}{p}}}{n^{\frac{1}{4} - \frac{1}{2p} - \frac{1}{2s} + \frac{1}{ps}}} \right)^{\frac{1}{1 - \frac{1}{s} - \frac{1}{p}}} \log(n)^2,$$

which means the discrete STFT of a NSN time series can be well approximated by its Gaussian companion under mild conditions.

4. ROBUSTNESS OF SIGNAL RECONSTRUCTION BY SST

To establish uncertainty quantification of TFRs determined by STFT and SST, we require an algorithm capable of accurately recovering the underlying oscillatory signal that satisfies the AHM. To this end, we consider a reconstruction algorithm based on SST and aim to demonstrate the robustness of SST-based signal reconstruction under the AHM framework.

Recall that when $\mathbf{h}(0) \neq 0$, the SST-based reconstruction formula [32] for recovering an oscillatory component $f(t) = A(t) \cos(2\pi\phi(t))$, which satisfies the AHM, from a noisy observation $Y = f + \Phi$, where Φ is a tempered distributed random process modeling the noise [3, 25], is defined as

$$(22) \quad \check{f}^{\mathbf{C}}(t) := \frac{1}{\mathbf{h}(0)} \int_{\xi \in R_t} S_Y^{(\mathbf{h})}(t, \xi) d\xi,$$

where $R_t := [-\Delta_r, \Delta_r] + \check{\phi}'(t)$, $\check{\phi}'(t)$ is the estimated $\phi'(t)$, with $\Delta_r > \varepsilon^{1/3}$ a small constant chosen by the user. Note that in the literature [8, 3], R_t is defined with $\Delta_r = \varepsilon^{1/3}$ when $\varepsilon > 0$. To handle the degenerate case that $\varepsilon = 0$, we modify the reconstruction formula and consider a non-degenerate Δ_r . In practice, $\check{\phi}'(t_l)$ can be estimated using ridge extraction algorithms applied to the TFR derived from the STFT [15] or the SST [3]. See [16] for further details and existing results on ridge analysis within the TFR framework. It is important to note that while several empirically robust and accurate ridge extraction algorithms have been developed, the theoretical analysis of their accuracy in estimating the IF from the TFR, particularly when noise exists, remain an open question. Therefore, in the analysis below, we assume that the ridge extraction algorithm is sufficiently accurate and replace $\check{\phi}'(t)$ by $\phi'(t)$. Estimating ε from a given time series is fundamentally a model selection problem. Empirically, overestimating ε does not appear to cause significant harm. To the best of our knowledge, this remains an unexplored area. Addressing the challenges of how accurately $\check{\phi}'(t)$ estimates $\phi'(t)$ and how to obtain ε from the time series lies beyond the scope of the present work and will be explored in our future research; however, we refer the reader to [16] for a recent effort in the direction of ridge extraction, which also includes a review of existing methods.

In practice, we discretize (22) directly to analyze a sampled version of Y or a time series, an approach commonly adopted in applications (also see, e.g., [33, 19], among others). While pointwise robustness for a similar reconstruction formula based on the continuous wavelet transform has been established in [3], to our knowledge, no robustness results are available for (22) under general nonstationary noise, let alone uniform robustness.

To establish the desired robustness result, we model the observed time series Y_i as a discretization of an oscillatory component f satisfying the AHM and Assumption 2.1, with additive mean-zero nonstationary noise conforming to the NSN model. That is, $Y_i = f_i + \sigma\epsilon_i$, as defined in (11). Following the discretization scheme (13), we sample the signal at a rate $q = \sqrt{n}$ Hz and collect n observations. The corresponding Nyquist rate is $\sqrt{n}/2$, which exceeds Ξ when n is sufficiently large. Set $m = \lceil \beta q \rceil \asymp \sqrt{n}$. We then discretize (22) as follows. First, the continuous STFT is numerically implemented via the discretized STFT $V_Y^{(\mathbf{h})}(t_l, \eta_j)$ defined in (5) at time t_l and frequency $\eta_j = j\Xi/d$, where $j = 1, \dots, d$, and $d \in \mathbb{N}$ denotes the number of frequency bins. Next, the SST is computed as $S_Y^{(\mathbf{h})}(t_l, \xi_k)$ according to (9), where $C = \Xi$, $\xi_k = k\Xi/d$ for $k = 1, \dots, d$ and the threshold $\nu \geq 0$. Finally, the

SST reconstruction formula with the threshold $\nu \geq 0$ is implemented by

$$(23) \quad \tilde{f}^{\mathbb{C}}(t_l) := \frac{1}{\mathbf{h}(0)} \frac{\Xi}{d} \sum_{\xi_k \in R_l} S_Y^{(\mathbf{h})}(t_l, \xi_k),$$

which is clearly a direct discretization of (22).

It is well known in practice that when d is sufficiently large and $\epsilon = 0$; that is, in the absence of noise, the oscillatory signal f can be accurately recovered via the discrete reconstruction formula $\tilde{f}^{\mathbb{C}}$, as it approximates the continuous version $\tilde{f}^{\mathbb{C}}$. However, to the best of our knowledge, a rigorous justification of this approximation in the discrete setting remains unavailable in the literature. Below, we show that in the presence of noise, if we properly choose d , the reconstruction formula $\tilde{f}^{\mathbb{C}}$ remains accurate, yielding a uniform error bound in l and with high probability. This result also answers the case when the signal is noise-free when $\sigma \rightarrow 0$.

To state the robustness result, we impose the following assumption about the window function.

Assumption 4.1. Let \mathbf{h}_0 be a nonnegative and symmetric Schwartz function that is compactly supported on $[-1, 1]$ and normalized to have unit L^2 norm. Assume the Fourier transform of \mathbf{h}_0 , denoted as $\hat{\mathbf{h}}_0$, satisfies $|\hat{\mathbf{h}}_0(\eta)| > \delta_1$ on $[-\Delta_0, \Delta_0]$, where $\delta_1 > 0$ and $\Delta_0 > 1$, and $\int_{\Delta_0}^{\infty} |\hat{\mathbf{h}}_0(\eta)| d\eta \leq \delta_2$, where $\delta_2 > 0$ is a small constant. Take $\beta > 0$ so that $\Delta := \Delta_0/\beta < \Xi_s/2$ and define $\mathbf{h}(t) = \mathbf{h}_0(t/\beta)/\sqrt{\beta}$.

The parameters δ_1 and δ_2 are jointly used to describe the shape of a window function \mathbf{h} . Due to the Schwartz condition, the Fourier transform of \mathbf{h} decays faster than any polynomial. Consequently, we can choose Δ_0 to be of order 1, ensuring that both δ_1 and δ_2 remain small. As we will see below, these parameters quantify the reconstruction accuracy. It is therefore desirable to design window functions with small values of δ_1 and δ_2 . Recall that for any $\delta \in (0, 1)$ and any $C > 0$, there exists a real, nonnegative and symmetric Schwartz function h that is supported in $[-1, 1]$, so that $C_1 e^{-(1+\epsilon)C\xi^\delta} \leq \hat{h}(\xi) \leq C_2 e^{-(1-\epsilon)C\xi^\delta}$ for any small $\epsilon > 0$ and some $C_1, C_2 > 0$ [29]. For such a kernel function, we can choose $\delta_1 = C_1 e^{-(1+\epsilon)C\Delta_0^\delta}$ and $\delta_2 = \frac{C_2}{(1-\epsilon)C\delta} e^{-(1-\epsilon)C\Delta_0^\delta}$. On the other hand, the parameter β controls the spectral concentration of the window \mathbf{h} , helping to mitigate spectral interference. This is particularly important since the signal under consideration is real. This setup reflexes the common practice of using a wider window for analyzing lower-frequency signals. Note that β scales with Δ_0 , and we need a larger Δ_0 to achieve smaller δ_1 and δ_2 . In this case we typically need a larger β .

While the conditions in this Assumption can be relaxed, such as considering non-compact or low regularity or wavelet-like windows, doing so would require more cumbersome notation without yielding additional insight relevant to our analysis. For the sake of clarity and simplicity, we retain these assumptions. In general, Δ_r in the reconstruction formula (22) is much smaller than Δ since the TFR concentration has been enhanced by the SST.

The robustness result of the reconstruction formula is stated in following theorem, and the proof is postponed to Section A.4.

Theorem 4.2. Suppose Y_i follows model (11), where $f_i = f(t_i)$, $t_i = i/\sqrt{n}$, and f satisfies the AHM with Assumption (2.1) fulfilled, and ϵ_i satisfies the NSN model and Assumption 2.2, with the condition $A > \sqrt{\chi} + 1$ fulfilled. Set $m = \lceil \beta\sqrt{n} \rceil$,

$d = n^{1/3-\gamma}$, and $\sigma = \sigma(n) = n^{1/4-\gamma'}$, where $\gamma, \gamma' > 0$ are small constants. Set the frequency domain sampling points as $\eta_k = \frac{k\Xi}{d}$, where $k = 1, \dots, d$. Suppose the window function \mathbf{h} satisfies Assumption 4.1 and Δ is chosen properly so that $\frac{2(E_f' + \Xi E_f)}{\Xi_a \sqrt{\beta} \delta_1} \leq 1/2$, where E_f and E_f' are defined in Lemma A.3. Set the parameters for SST as $\alpha := (\Delta_r/C_\alpha)^2$ for some $C_\alpha > 1$, and $\nu := \Xi_a \sqrt{\beta} \delta_1/2 + \zeta_n$, where $\zeta_n \asymp n^{-\gamma'} \sqrt{\log n}$ is specified in (52). Then, when $\varepsilon \geq 0$ is sufficiently small and n is sufficiently large, with probability greater than $1 - n^{-2}$, the SST reconstruction formula with the threshold $\nu/2$ satisfies

$$(24) \quad \max_{l=m+1, \dots, n-m} \left| \tilde{f}^{\mathbf{C}}(t_l) - A(t_l) e^{i2\pi\phi(t_l)} \right| \leq C_1 \Xi_A + C_2 \zeta_n,$$

where $C_1 > 0$ is a small constant comprises of terms linearly depending on $\delta_1, \delta_2, \varepsilon$ and $\operatorname{erfc}(C_\alpha)$ respectively, $\operatorname{erfc}(\cdot)$ is the complementary error function, and $C_2 > 0$, which might not be small. Details of C_1 and C_2 can be found in (60).

Note that the maximum is evaluated over indices from $m+1$ to $n-m$, which is intentionally designed to mitigate boundary effects. Near the boundaries, only portions of the window function are supported, leading to lower quality reconstruction. Addressing boundary effects is an independent topic of interest; for instance, one possible approach is to forecast the signal prior to applying the algorithm [20]. While the boundary effect needs to be handled, like in the applications that real-time decision making is critical, boundary effects are asymptotically negligible in many applications. Thus, we report results without explicitly addressing them in order to maintain the focus of the paper.

The noise level, modeled as $\sigma \epsilon_i$ with $\sigma = \sigma(n) = n^{1/4-\gamma'}$, may appear surprising at first glance, as it suggests that the noise amplitude grows asymptotically. However, as shown in the proof, the standard deviation of $V_\epsilon^{(\mathbf{h})}(t_l, \xi_k)$ is of order $n^{-1/4}$ up to a logarithmic factor. Thus, the scaling by σ adjusts the standard deviation of the TFR to be of order 1 as a random field. This normalization aligns with the continuous framework adopted in [3], where the noise is modeled as a distributed random process Φ such that $\Phi(\mathbf{h})$ has a standard deviation of order 1. In this sense, our result extends the pointwise robustness analysis reported in [3] to a uniform one under the discrete setting. When $\gamma' = 1/4$, we obtain the intuitive case where the magnitude of the noise is bounded.

The reconstruction error comprises two main contributions. $C_1 \Xi_A$ comes from the AHM and window truncation in the reconstruction formula, specifically through the definition of R_l . The second term, $C_2 \zeta_n$, reflects the influence of the noise. Since E_f and E_f' in the constraint $\frac{2(E_f' + \Xi E_f)}{\Xi_a \sqrt{\beta} \delta_1} \leq 1/2$ depend linearly on Ξ_A , this constraint effectively imposes a lower bound on $\sqrt{\beta} \delta_1$, indicating that δ_1 cannot be chosen arbitrarily small. Consequently, even in the purely harmonic case where $\varepsilon = 0$, the term C_1 does not vanish. If we choose $\delta_2 = C_h \Delta \mathbf{h}(0) \beta \delta_1$, the error terms in C_1 can be simplified. In the absence of noise, that is, when $\epsilon_i = 0$, we have $C_2 \zeta_n = 0$, and the theorem reduces to the noise-free setting. In this case, the error scales linearly with Ξ_A .

The robustness of the IMT function retrieval via the SST-based reconstruction formula presented in this theorem also ensures the robustness of AM and phase reconstruction via SST; that is, we estimate A_l by $|\tilde{f}_l^{\mathbf{C}}|$, and the phase ω_l by unwrapping $\tilde{f}_l^{\mathbf{C}}/|\tilde{f}_l^{\mathbf{C}}|$, where the error is uniformly controlled accordingly.

5. UNCERTAINTY QUANTIFICATION OF SST BY BOOTSTRAPPING

In many real-world scenarios, an oscillatory component may or may not be present. For example, spindles in electroencephalogram (EEG) signals do not always occur. A priori, we do not know whether such oscillations exist or when they appear. Moreover, even if they do exist, their strength may be too weak and buried in noise. A critical task in applying SST is to determine whether an oscillatory component is present in a given signal and to quantify the associated uncertainty. In practice, obtaining the statistics of ϵ_i is challenging. However, when ϵ_i satisfies certain mild conditions, particularly the regularity of the filtration process, we can approximate it with a time-varying autoregressive (tvAR) process, ensuring that the deviation of its covariance structure from that of ϵ_i remains controlled [10]. Furthermore, our previously established Gaussian approximation result ensures that STFT of the tvAR process can be well approximated by that of a Gaussian tvAR process with the same model coefficients uniformly in time and frequency. As a result, intuitively the distributional behavior of the SST of ϵ_i can be well approximated by that of a Gaussian tvAR process. Based on those facts, we propose an algorithm to bootstrap the noise ϵ_i , assuming prior knowledge that the underlying data generating mechanism of $\{\epsilon_i\}$ is slowly varying in time; that is, it satisfies the locally stationary condition. Based on this bootstrap approach, we further develop algorithms to quantify the uncertainty in SST and establish a noise thresholding framework.

5.1. Bootstrap the noise. Suppose the given time series is $\{X_i\}_{i=1}^n$. Consider the null hypothesis that $f_i = 0$. First, if we are not sure if the null condition holds, apply SST to reconstruct the putative oscillatory component and denote the reconstructed component as \tilde{f}_i . Hence, obtain an estimate of the random noise via $\tilde{\epsilon}_i := X_i - \tilde{f}_i$. If we are sure that the null condition holds, set $\tilde{f}_i = 0$ and $\tilde{\epsilon}_i := X_i$.

Next, with $\tilde{\epsilon}_i$, we apply the following procedure to approximate the error process $\{\epsilon_n\}$ by a tvAR process $\{x_n\}$ with the short range dependence assumption satisfying

$$x_i = \sum_{j=1}^b \phi_j(i/n)x_{i-j} + \varepsilon_i,$$

where $\{\varepsilon_i\}$ is a locally stationary white noise process, $b \in \mathbb{N}$ is the order of the tvAR process and ϕ_j is a smooth function defined on $[0, 1]$ with proper conditions. To approximate ϕ_j , consider a proper orthonormal basis of a finite dimensional subspace of $L^2[0, 1]$, denoted as $\{\psi_i\}_{i=1}^m$; that is, assume $P_S \phi_j \approx \phi_j$ for $j = 1, \dots, b$, where $S := \text{span}\{\psi_i\}_{i=1}^m$ so that

$$x_i \approx \sum_{j=1}^b \sum_{k=1}^m a_{ik} \psi_j(i/n)x_{i-j} + \varepsilon_i.$$

By a direct linear regression we could estimate a_{ik} from $\{\tilde{\epsilon}_i\}_{i=1}^n$ so that

$$\tilde{\phi}_j(i/n) = \sum_{k=1}^m \tilde{a}_{ik} \psi_j(i/n).$$

The innovation process associated with the tvAR process approximation is estimated via

$$\tilde{\varepsilon}_i := x_i - \sum_{j=1}^b \tilde{\phi}_j(i/n) \tilde{\varepsilon}_{i-j}$$

when $i = b + 1, \dots, n$ and when $i = 1, \dots, b$ we could simply set $\tilde{\varepsilon}_i = \tilde{\varepsilon}_i$ or estimate it by the reverse process. The time-varying standard deviation of the estimated innovation process is estimated by a moving averaging process; that is

$$\tilde{\sigma}_i = \text{STD}\{\tilde{\varepsilon}_j, \max\{1, i - I\} \leq j \leq \min\{n, i + I\}\},$$

where $I \in \mathbb{N}$ is chosen to be 20 in practice but can be optimized. This naive moving averaging approach can be replaced by a more sophisticated approach. To bootstrap the locally stationary random process $\{\varepsilon_i\}$, for each $m = 1, \dots, M$, we generate a random process, $\{\varepsilon_i^{(*m)}\}$, in the following way. Take an i.i.d. Gaussian random process $\eta_i^{(*m)}$ with mean 0 and standard deviation 1. Set

$$\varepsilon_i^{(*m)} := \begin{cases} \tilde{\sigma}_i \eta_i^{(*m)} & \text{when } i = 1, \dots, b \\ \sum_{j=1}^b \tilde{\phi}_j(i/n) \varepsilon_{i-j}^{(*m)} + \tilde{\sigma}_i \eta_i^{(*m)} & \text{when } i = b + 1, \dots, n \end{cases}$$

We now present a bootstrapping theorem under the locally stationary assumption. A random process $Z_j, j \in \mathbb{Z}$, is said to satisfy the *uniformly positive definite in covariance* (UPDC) condition if, for sufficiently large n , the smallest eigenvalue of the covariance matrix of (Z_1, \dots, Z_n) is bounded below by a positive constant $\kappa > 0$. Furthermore, if $\max_k |\text{cov}(Z_k, Z_{k+r})| \leq r^{-\tau}$ for all $r \in \mathbb{N}$ and some $\tau \geq 0$, we refer to τ as the *covariance decay speed*. We also refer to [10] for a more detailed description of covariance locally stationary time series, the UPDC and the short memory conditions, as well as some associated examples. The proof is postponed to Section A.5.

Theorem 5.1. Assume $\{\varepsilon_i\}_{i=1}^n$ is locally stationary and the associated covariance function is smooth, the local spectral density of ε_i is lower bounded and fulfills the UPDC condition, and ε_i satisfies a polynomial covariance decay rate $\tau > 2$. Moreover, assume conditions in Theorem 3.2 are satisfied. Then there exists a probability space associated with the bootstrapping, called $(\Omega, \mathcal{F}, \mathbb{P})$, where we could construct a Gaussian tvAR random process according to the procedures in Section 5.1, $\{\varepsilon_i^{(*)}\}_{i=1}^n$, established from $\{\varepsilon_i\}_{i=1}^n$. Take d frequencies, $\mathcal{G} := (\xi_1, \dots, \xi_d)$, where $d = n^a$ and $a \geq 0$. Then, when

$$a = \min \left\{ \gamma, \frac{\frac{1}{4} - \frac{1}{2p} - \frac{1}{2s} + \frac{1}{ps}}{\frac{5}{4} - \frac{1}{s} - \frac{3}{2p}} \right\} - \vartheta,$$

where ϑ is any small positive constant so that $a \geq 0$, $\gamma = \frac{\tau-2}{\tau+1} \in (0, 1]$ and b is chosen to fulfill $\frac{b}{\log(b)} \asymp n^{1/(\tau+1)}$, we have

$$\max_{l=1, \dots, d} \max_{i=1, \dots, n} \left| S_{\varepsilon}^{(\mathbf{h})}(t_i, \xi_l) - S_{\varepsilon^{(*)}}^{(\mathbf{h})}(t_i, \xi_l) \right| = o_p(1).$$

When ε_i satisfies $p, s \rightarrow \infty$ and γ is close to 1, the exponent a approaches $1/5$. This rate is slightly worse than the Gaussian approximation for STFT, as we used crude bounds to control the approximation error to simplify the proof. According to [25], if we further assume that ε_i is stationary, $S_{\varepsilon^{(*)}}^{(\mathbf{h})}(t_i, \xi_l)$ is complex Gaussian

with nontrivial variation. Therefore, $\max_{l=1,\dots,d} \max_{i=1,\dots,n} \left| S_\epsilon^{(\mathbf{h})}(t_i, \xi_l) \right|$ is away from zero, and the resulting error control is meaningful.

5.2. Application to uncertainty quantification of SST. The first application concerns quantifying the uncertainty of SST. Given the time series $\{X_i\}_{i=1}^n$, we run SST on $X^{(*m)} := \tilde{f}_i + \epsilon_i^{(*m)}$, $m = 1, \dots, M$, over a grid in the time-frequency domain, denoted by $\mathcal{G} := \{t_1, \dots, t_{n'}\} \times \{\xi_1, \dots, \xi_d\} \subset \mathcal{S} := \{1/\sqrt{n}, 2/\sqrt{n}, \dots, \sqrt{n}\} \times \{1/\sqrt{n}, \dots, \sqrt{n}/2\}$, where d is guided by Theorem 5.1. Clearly, \mathcal{S} is the full grid that hosts n sample points in the time domain and $n/2$ canonical frequencies in the frequency domain. In practice, we set $n' = n$ and $t_l = l/\sqrt{n}$ in \mathcal{G} , or if we aim to speed up the algorithm, a sparser grid can be chosen. At each point in \mathcal{G} , we compute the empirical $(\alpha/2)$ -th and $(1 - \alpha/2)$ -th percentiles, where $\alpha > 0$ is chosen by the user, based on the M realizations, $\{|S_{X^{(*m)}}^{(\mathbf{h})}(t_j, \xi_k)|\}_{m=1}^M$. These percentiles are then interpolated from \mathcal{G} to the full grid \mathcal{S} using cubic splines. Denote the resulting interpolated function as $|S|_{X, \alpha/2} \in \mathbb{R}^{n \times \lfloor n/2 \rfloor}$ and $|S|_{X, 1-\alpha/2} \in \mathbb{R}^{n \times \lfloor n/2 \rfloor}$. Plotting $|S|_{X, \alpha/2}$ and $|S|_{X, 1-\alpha/2}$ alongside $|S_X^{(\mathbf{h})}|$ provides a visual representation of the uncertainty of SST in the presence of noise contamination by ϵ_i . See Figure 5 for a simulation with $\alpha = 0.05$ and Section 6 for details.

The second application focuses on noise thresholding. We run SST on $\epsilon_i^{(*m)}$, $m = 1, \dots, M$, over the grid \mathcal{G} . At each point in \mathcal{G} , we estimate a threshold corresponding to a user-specified $(1 - \alpha)$ confidence level, where $\alpha > 0$ is chosen by the user. This threshold is then interpolated to the full grid \mathcal{S} and denoted as $T \in \mathbb{R}^{n \times \lfloor n/2 \rfloor}$. We then threshold the SST coefficients of X_i by setting coefficients below the threshold to zero. The resulting thresholded TFR, denoted as $S_{X,T}^{(\mathbf{h})} \in \mathbb{R}^{n \times \lfloor n/2 \rfloor}$, is given by

$$S_{X,T}^{(\mathbf{h})}(i, k) := S_X^{(\mathbf{h})}(t_i, \xi_k) I(|S_X^{(\mathbf{h})}(t_i, \xi_k)| \geq T(i, k)).$$

where $I(\cdot)$ is the indicator function. A similar bootstrapping procedure can be applied to quantify the uncertainty of the STFT and to determine appropriate thresholds.

6. NUMERICAL SIMULATION

6.1. Null case. To numerically validate this result, fix $n = 2048$, and construct a locally stationary random process in the following way. First, construct a tvAR process via

$$\epsilon_i = \begin{cases} \eta_i & \text{when } i = 1, 2 \\ \sum_{k=1}^2 \phi_k(i/n) \epsilon_{i-k} + \eta_i & \text{when } i = 3, 4, \dots, n \end{cases}$$

where η_i is an i.i.d. Gaussian process with standard deviation 1, $\phi_1(i) = -0.5(0.7 + 0.3 \cos(2\pi i/n))$ and $\phi_2(i) = 0.3\sqrt{0.1 + i/(4n)}$. Then, construct the simulated locally stationary random process via $x_i = (1 + 0.5 \cos(2\pi i/n)) \epsilon_i$. See Figure 1 for an illustration of the estimated tvAR process and one realization of the bootstrap time series.

The true distributions of STFT and SST are collected by realizing x_i for $M = 1000$ times, and the bootstrapped distributions are generated from realizing 1000 bootstraps of one realization of x_i . See Figures 7 and 8 in the Supplementary for the QQ plots comparing the distributions of the STFT and SST coefficients under the true noise model and those obtained via bootstrapping, evaluated at various

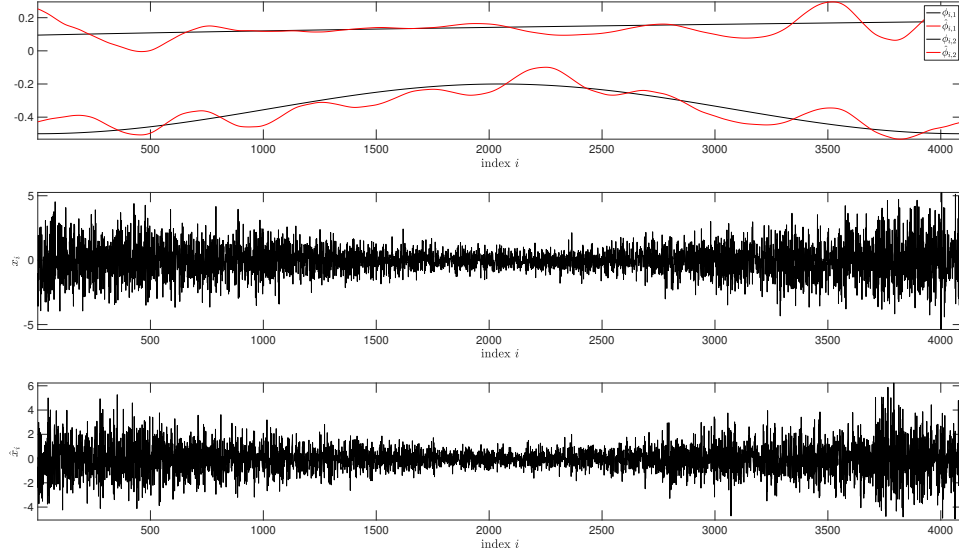


FIGURE 1. Top: the true tvAR coefficients, and the estimated coefficients of the approximate tvAR process. Middle: one realization of x_i . Bottom: the bootstrapped x_i .

time-frequency pairs. We can see that numerically the bootstrapping approach provides satisfactory results.

6.2. Non-null case. We assume the knowledge of the number of oscillatory components and apply the following algorithm for bootstrap. First, we generate simulated oscillatory signals in the following way. Consider a standard Brownian motion B_i indexed by i , where $i = 1, \dots, n$, and smoothen it by convolving it with a chosen kernel K with a support of 700 points. Denote the resulting random process by b_i and obtain $A(i/\sqrt{n}) := 3 + b_i/\|b_i\|_{\ell_\infty}$. Note that $\sqrt{n} > 0$ is the sampling rate. Similarly, construct a monotonically increasing function by taking another standard Brownian motion B'_i , $i = 1, \dots, n$, that is independent of B_i and smoothen it with a chosen kernel K' with a support of 500 points. Denote the resulting random process by p_i . Construct $\phi'(i/\sqrt{n}) := 4 + \frac{0.5i}{17\sqrt{n}} + 1.2\frac{p_i}{\|p_i\|_{\ell_\infty}}$. The monotonic random process, denoted as $\phi(i/\sqrt{n})$, is obtained via normalized cumsum; that is, $\phi(i/\sqrt{n}) = \frac{1}{\sqrt{n}} \sum_{j=1}^i \phi'(j/\sqrt{n})$. The oscillatory signal is constructed by $f(i/\sqrt{n}) := A(i/\sqrt{n}) \cos(2\pi\phi(i/\sqrt{n}))$. Clearly, $A(i/\sqrt{n})$, $\phi'(i/\sqrt{n})$ and $\phi(i/\sqrt{n})$ are the AM, IF and phase of the oscillatory signal sampled at i/\sqrt{n} second. This construction of oscillatory signal is in practice closer to real world data and has been considered in various time-frequency analysis literature. The noise ϵ_i is constructed by the same way as that in the null case, so that the final non-null random process is $X_i := f(i/\sqrt{n}) + \epsilon_i$.

With one realization of the simulated signal, we reconstruct the oscillatory components, denoted as $\tilde{f}(i/\sqrt{n})$, using the SST-based reconstruction formula and subtract it from the signal to get the reconstructed noise, denoted as $\tilde{\epsilon}_i$. Then, bootstrap the noise on $\tilde{\epsilon}_i$ for $M \geq 1$ times, denoted as $\epsilon_i^{(*m)}$, where $m = 1, \dots, M$.

Set $M = 1000$. The noisy signal and the reconstructed deterministic signal, and the associated TFRs are shown in Figure 2. With the reconstructed noise, the bootstrap result is shown in Figure 3. The QQ plots of distributions of STFT and SST of true noise and bootstrapped noise are shown in Figures 9 and 10 respectively. The result supports the validity of combining SST-based reconstruction with the bootstrap approach.

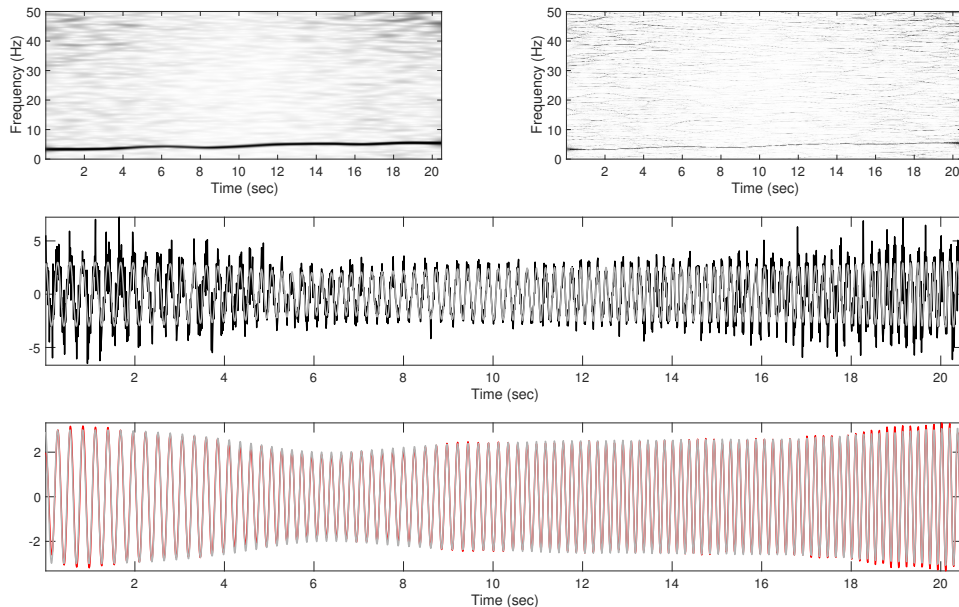


FIGURE 2. Top left: the STFT of the noisy signal. Top right: the SST of the noisy signal. Middle: one realization of noisy signal (black) and the true deterministic signal (gray). Bottom: reconstructed deterministic signal (red) and the true deterministic signal (gray).

The bootstrap-based uncertainty quantification results are shown in Figure 4. We generate bootstrapped signals, denoted as $x_i^{(*m)} := \tilde{f}(i/\sqrt{n}) + \epsilon_i^{(*m)}$, where $m = 1, \dots, 1000$, and run SST on $\hat{x}_i^{(*m)}$. Set significance level $\alpha = 0.05$. Figure 4(d) displays the TFR of the noisy signal shown in Figure 4(a). Figures 4(b) and (c) present the lower and upper bounds of the 95% confidence interval. $|S|_{X,0.025}$ and $|S|_{X,0.975}$ respectively, computed using the true signal and 1000 realizations of the true noise. In Figures 4(e) and (f), we show the corresponding confidence bounds derived from the 1000 bootstrapped samples, based on the reconstructed signal and resampled noise. Notably, the bootstrap-based intervals closely match those obtained from the true model. While a faint curve around 4 Hz, which corresponds to the true IF, is visible in the noisy TFR in Figure 4(d), its existence remains ambiguous. However, with the aid of the confidence intervals shown in Figures 4(e) and (f), the curve becomes clearly distinguishable. Assessing how accurately this curve reflects the true IF pertains to the ridge extraction problem, which lies beyond the scope of this paper and will be addressed in future work.

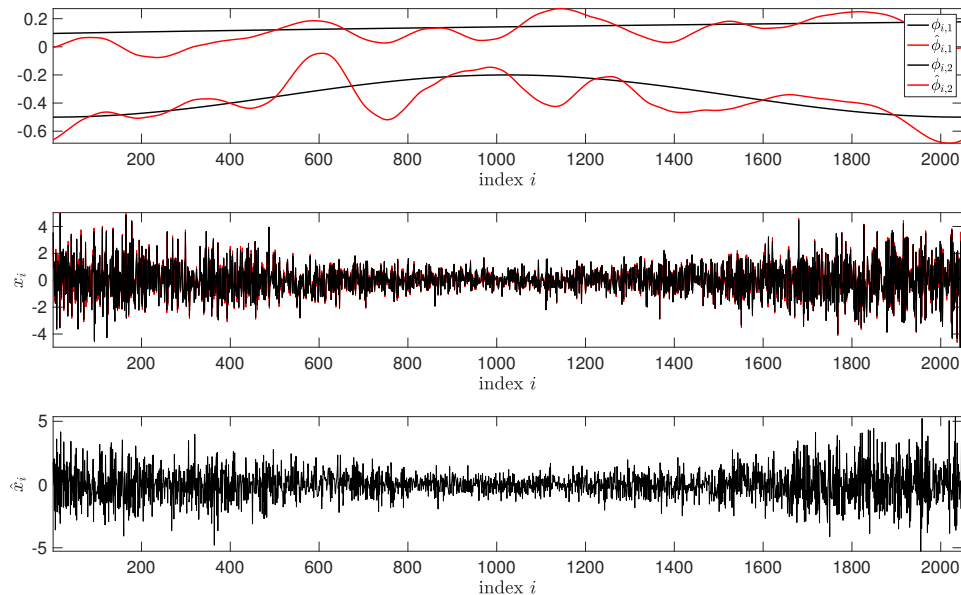


FIGURE 3. Top: the true tvAR coefficients, and the estimated coefficients of the approximate tvAR process. Middle: one realization of x_i and the reconstructed x_i . Bottom: the bootstrapped x_i .

See Figure 5 for the results of noise thresholding, where the threshold is determined based on the 95th percentile of the bootstrapped noise values, $\{\epsilon_i^{(*m)}\}_{i=1}^n$, for $m = 1, \dots, 1000$, under the null hypothesis. In the TFRs of the noisy signal obtained via STFT and SST (Figures 5(a) and (d), respectively), background speckles are visible, particularly around 0-5 s and 15-20 s above 10 Hz, which are attributable to noise. Using bootstrapped uncertainty quantification from pure noise TFRs, we obtain a statistically reliable threshold (Figures 5(b) and (e)). Applying this threshold results in cleaner TFRs (Figures 5(c) and (f)), in which noise-induced speckles are effectively suppressed. The denoising effect is especially prominent in the SST.

6.3. Application to sleep spindle analysis. Sleep spindles are brief bursts of activity in the sigma frequency range (around 11-16 Hz) of the electroencephalogram (EEG) signal, lasting 0.5 to 2 seconds [14]. They are characteristics of the N2 stage of non-rapid eye movement sleep, marking the transition between light and deep sleep. Understanding sleep spindles is key to decoding sleep architecture, memory consolidation, and cognitive functions, and can shed light on healthy sleep patterns and neurological disorders [30]. Notably, spindle frequencies vary and are characterized by IF. The absence of spindle deceleration is linked to disorders like sleep apnea and autism in children [2, 26]. Inter-expert agreement on spindle identification is limited, but reliability can be improved using qualitative confidence scores [31]. Estimating spindle duration is particularly challenging due to the thin-tail structure of spindles. A nonlinear multitaper method, a variation of SST called concentration of frequency and time (ConceFT), has been shown efficient in handling this issue [24]. We conjecture that our proposed bootstrap algorithm could

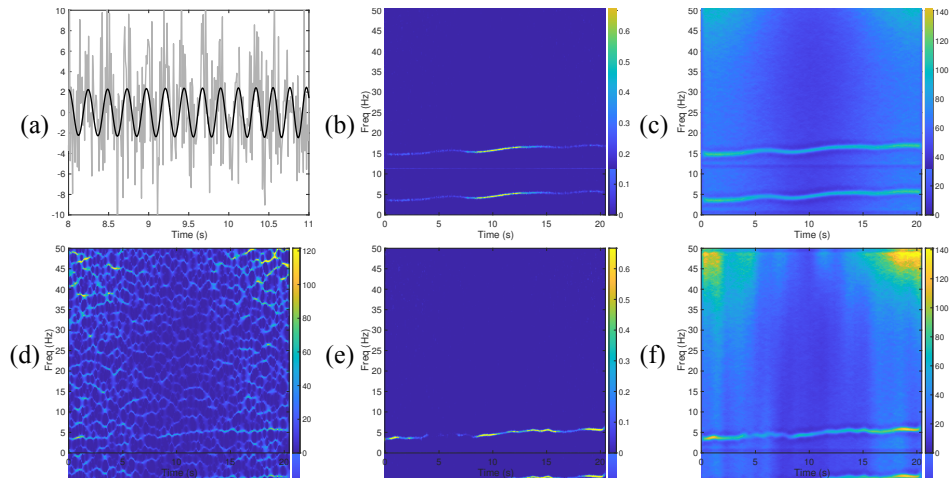


FIGURE 4. Results of uncertainty quantification. (a) a 3 second segment of the noisy signal is shown in gray with the clean signal superimposed in black. (b) and (c) TFRs of pointwise 95% confidence interval with realizing the random process 1000 times, where (b) is the 2.5% percentile plot, and (c) is the 97.5% percentile plot. (d) the TFR of the noisy signal. (e) and (f) TFRs of pointwise 95% confidence interval determined from 1000 bootstrapped noises and the reconstructed signal, where (b) is the 2.5% percentile plot, and (c) is the 97.5% percentile plot.

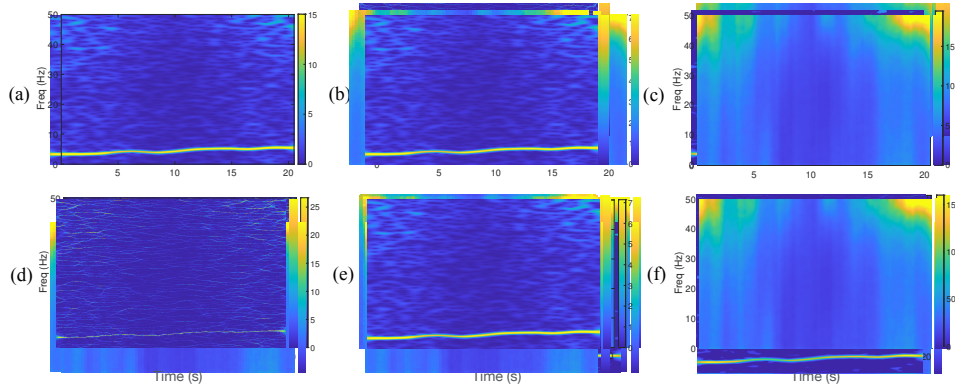


FIGURE 5. Results of thresholding noise. (a) the STFT of a nonnull signal. (b) 95% percentile of the bootstrapping with $M = 1000$ as the threshold, with interpolation to the whole grid. (c) after thresholding. (d) the SST of a nonnull signal. (e) 95% percentile of the bootstrapping with $M = 1000$ as the threshold, with interpolation to the whole grid. (f) after thresholding.

help handle this challenge and provide quantitative confidence. We show how the proposed bootstrap algorithm works on a segment from the open-access DREAMS database [9]. Figure 6 shows the spectrogram, SST, and threshold determined by

the 95th percentile of the noise distribution via the bootstrap algorithm. The red bars indicate spindles identified by experts. In the spectrogram, spindle dynamics, especially the IF, are difficult to discern. However, the dynamics, particularly the IF, can be visualized in the SST as curves. Both labeled spindles show decreasing IFs. The thresholding further clarifies the TFR, reducing background noise and revealing clear IF traces. Although not labeled, there is likely a spindle in the first 2 seconds with increasing, nonlinear IF dynamics. Given the raw EEG signal's complexity, it is understandable why this spindle was missed in expert's label—it overlaps with a bump and does not resemble a typical spindle. The conjecture that the uncertainty quantification of SST could assist expert annotation, and the question if it can help explore spindle dynamics, will be explored in future work.

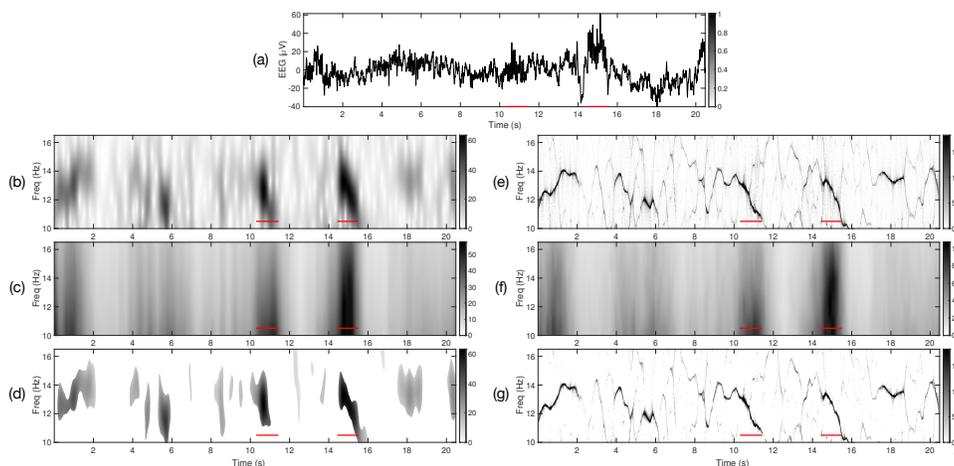


FIGURE 6. An illustration of spindle analysis using the proposed bootstrapping algorithm. (a) the EEG signal recorded during the N2 sleep stage. (b)-(d): the spectrogram, the threshold determined by the 95% percentile of noise distribution determined by the bootstrap algorithm, and the thresholded time-frequency representation (TFR). (e)-(g): the synchrosqueezing transform, the threshold determined by the 95% percentile of noise distribution determined by the bootstrap algorithm, and the thresholded TFR.

REFERENCES

- [1] P. Billingsley. *Convergence of Probability Measures*. John Wiley & Sons, 1968.
- [2] D. Z. Carvalho, G. J. Gerhardt, G. Dellagustin, E. L. de Santa-Helena, N. Lemke, A. Z. Segal, and S. V. Schönwald. Loss of sleep spindle frequency deceleration in obstructive sleep apnea. *Clinical Neurophysiology*, 125(2):306–312, 2014.
- [3] Y.-C. Chen, M.-Y. Cheng, and H.-T. Wu. Nonparametric and adaptive modeling of dynamic seasonality and trend with heteroscedastic and dependent errors. *J Roy Stat Soc B*, 76(3):651–682, 2014.

- [4] V. Chernozhukov, D. Chetverikov, and K. Kato. Gaussian approximations and multiplier bootstrap for maxima of sums of high-dimensional random vectors. *Ann. Statist.*, 41:2786–2819, 2013.
- [5] V. Chernozhukov, D. Chetverikov, and K. Kato. Comparison and anti-concentration bounds for maxima of gaussian random vectors. *Probab. Theory Relat. Fields*, 162:47–70, 2015.
- [6] M. Csörgő and P. Révész. A new method to prove strassen type laws of invariance principle. I. *Zeitschrift für Wahrscheinlichkeitstheorie und verwandte Gebiete*, 31(4):255–259, 1975.
- [7] R. Dahlhaus. Fitting time series models to nonstationary processes. *Ann. Stat.*, 25(1):1–37, 1997.
- [8] I. Daubechies, J. Lu, and H.-T. Wu. Synchrosqueezed wavelet transforms: an empirical mode decomposition-like tool. *Appl Comput Harmon A*, 30(2):243–261, 2011.
- [9] S. Devuyst. The DREAMS databases and assessment algorithm.
- [10] X. Ding and Z. Zhou. Autoregressive approximations to nonstationary time series with inference and applications. *Ann. Stat.*, 51(3):1207–1231, 2023.
- [11] R. Eldan, D. Mikulincer, and A. Zhai. The clt in high dimensions. *The Annals of Probability*, 48(5):2494–2524, 2020.
- [12] P. Flandrin. *Explorations in time-frequency analysis*. Cambridge University Press, 2018.
- [13] M. G. Genton and P. Hall. Statistical inference for evolving periodic functions. *J. Roy. Stat. Soc. B*, 69(4):643–657, 2007.
- [14] C. Iber, S. Ancoli-Israel, A. Chesson, and S. Quan. *The AASM manual for the scoring of sleep and associated events: rules, terminology, and technical specification*. Westchester, IL: American Academy of Sleep Medicine, 2007.
- [15] N. Laurent and S. Meignen. A novel ridge detector for nonstationary multicomponent signals: Development and application to robust mode retrieval. *IEEE Trans. Signal Process*, 69:3325–3336, 2021.
- [16] G.-R. Liu, Y.-C. Sheu, and H.-T. Wu. Analyzing scalogram ridges in the presence of noise. *submitted. arXiv preprint arXiv:2501.00270*, 2024.
- [17] M. Liu, J. Yang, and Z. Zhou. Wasserstein and convex gaussian approximation for nonstationary time series of diverging dimensionality. *submitted*, 2025.
- [18] W. Liu, H. Xiao, and W. B. Wu. Probability and moment inequalities under dependence. *Statistica Sinica*, pages 1257–1272, 2013.
- [19] Y.-L. Lo, H.-T. Wu, Y.-T. Lin, H.-P. Kuo, and T.-Y. Lin. Hypoventilation patterns during bronchoscopic sedation and their clinical relevance based on capnographic and respiratory impedance analysis. *J. Clin. Monit. Comput.*, 34(1):171–179, 2020.
- [20] A. Meynard and H.-T. Wu. An efficient forecasting approach to reduce boundary effects in real-time time-frequency analysis. *IEEE T Signal Proces*, 69:1653–1663, 2021.
- [21] F. Mies and A. Steland. Sequential Gaussian approximation for nonstationary time series in high dimensions. *Bernoulli*, 29(4):3114 – 3140, 2023.
- [22] F. Móricz. Moment inequalities and the strong laws of large numbers. *Zeitschrift für Wahrscheinlichkeitstheorie und verwandte Gebiete*, 35(4):299–314, 1976.
- [23] S. Portnoy. On the central limit theorem in $r p$ when $p \rightarrow \infty$. *Probability theory and related fields*, 73(4):571–583, 1986.
- [24] R. Shimizu and H.-T. Wu. Unveil sleep spindles with concentration of frequency and time (concept). *Physiological Measurement*, 45(8):085003, 2024.
- [25] M. Sourisseau, H.-T. Wu, and Z. Zhou. Asymptotic analysis of synchrosqueezing transform—toward statistical inference with nonlinear-type time-frequency analysis. *Ann. Stat.*, 50(5):2694–2712, 2022.
- [26] S. Tessier, A. Lambert, M. Chicoine, P. Scherzer, I. Soulières, and R. Godbout. Intelligence measures and stage 2 sleep in typically-developing and autistic children. *Int. J. Psychophysiol.*, 97(1):58–65, 2015.
- [27] G. Thakur, E. Brevdo, N. S. Fučkar, and H.-T. Wu. The synchrosqueezing algorithm for time-varying spectral analysis: robustness properties and new paleoclimate applications. *Signal Processing*, 93(5):1079–1094, 2013.
- [28] G. Thakur and H.-T. Wu. Synchrosqueezing-based recovery of instantaneous frequency from nonuniform samples. *SIAM J. Math. Anal.*, 43(5):2078–2095, 2011.
- [29] T. Tlas. Bump functions with monotone fourier transforms satisfying decay bounds. *Journal of Approximation Theory*, 278:105742, 2022.

- [30] O. M. Weiner and T. T. Dang-Vu. Spindle oscillations in sleep disorders: a systematic review. *Neural plasticity*, 2016(1):7328725, 2016.
- [31] S. L. Wendt, P. Welinder, H. B. Sorensen, P. E. Peppard, P. Jennum, P. Perona, E. Mignot, and S. C. Warby. Inter-expert and intra-expert reliability in sleep spindle scoring. *Clinical Neurophysiology*, 126(8):1548–1556, 2015.
- [32] H.-T. Wu. *Adaptive analysis of complex data sets*. PhD thesis, Princeton University, 2011.
- [33] H.-T. Wu, S.-S. Hseu, M.-Y. Bien, Y. R. Kou, and I. Daubechies. Evaluating physiological dynamics via synchrosqueezing: Prediction of ventilator weaning. *IEEE Trans. Biomed. Eng.*, 61(3):736–744, 2013.
- [34] H.-T. Wu and Z. Zhou. Frequency detection and change point estimation for time series of complex oscillation. *J. Am. Stat. Assoc.*, 119(547):1945–1956, 2024.
- [35] H. Yang. Statistical analysis of synchrosqueezed transforms. *Applied and Computational Harmonic Analysis*, 45(3):526–550, 2018.
- [36] J. Yang and Z. Zhou. Spectral inference under complex temporal dynamics. *J. Am. Stat. Assoc.*, 117(537):133–155, 2022.
- [37] Z. Zhou. Heteroscedasticity and autocorrelation robust structural change detection. *J. Am. Stat. Assoc.*, 108(502):726–740, 2013.
- [38] Z. Zhou. Inference of weighted v-statistics for nonstationary time series and its applications. *Ann. Statist.*, 42:87–114, 2014.

APPENDIX A. PROOFS

A.1. Proof of Theorem 3.1: Sequential Gaussian approximation under HDNS. The main technical tool we need is a recently developed high-dimensional Gaussian approximation [17] for HDNS time series that generalizes results in [21], which is based on the martingale embedding technique [11]. The following theorem is a generalization of [21, Theorem 2.1].

Theorem A.1. [17, Theorem 3.2] Suppose the d -dimensional HDNS time series $\{z_i\}_{i=1}^n$ satisfy Assumption 2.2 with $A > \sqrt{\chi} + 1$. Consider $Z_n := \sum_{i=1}^n z_i \in \mathbb{R}^d$, and assume that the smallest eigenvalue of $\text{cov}(\frac{1}{\sqrt{n}}Z_n)$ is bounded below by some constant $\lambda_* > 0$. Then, on a sufficiently rich probability space, one can construct \hat{Z}_n such that $\hat{Z}_n \stackrel{D}{=} Z_n$ and a Gaussian random vector Y_n with the same mean and covariance matrix as Z_n . We have

$$(25) \quad \left\| \frac{1}{\sqrt{n}}(\hat{Z}_n - Y_n) \right\|_2 = O(dn^{1/s-1/2} \log(n)),$$

where $1/s := \max\left\{\frac{1}{p}, \frac{1}{\sqrt{\chi+1}p} + \left(\frac{1}{2} - \frac{1}{\sqrt{\chi+1}p}\right) \max\left\{\frac{2}{\sqrt{\chi+1}p}, \frac{1}{\chi} \left(\frac{1}{2} - \frac{1}{p}\right)\right\}\right\}$.

Note that the authors used the 2-Wasserstein distance in the statement of [17, Theorem 3.2], while in the proof it is the L^2 distance that is proved. When χ is sufficiently large, the convergence rate becomes $dn^{1/p-1/2}$, which is further reduced to $dn^{-1/2}$ when p is large. This allows us the nearly optimal convergence rate $d \asymp n^{1/2}$ [23].

We also need a generalized Rosenthal inequality for the HDNS model, as developed in [18, Section 4], which generalizes [18, Theorem 1] and is of independent interest. This result can also be viewed as a different version of [21, Theorem 3.2].

Lemma A.1 (Rosenthal inequality). Suppose the d -dimensional HDNS time series $\{z_i\}_{i=1}^n$ satisfy Assumption 2.2. Denote $S_i := \sum_{l=1}^i z_l$. Then, for $2 \leq p < \infty$, we have

$$(26) \quad \left\| \max_{1 \leq i \leq n} |S_i| \right\|_p \leq C\sqrt{dn},$$

where $C = C_p [\Theta_p(1) + B^{1/p}]$ for some constant C_p that depends only on p .

We establish some technical lemmas.

Lemma A.2. Under the same assumptions as those in Theorem A.1, denote $Z_{i,m} := \sum_{j=(i-1)m+1}^{im} z_i$, $i = 1, 2, \dots$, where $m = m(n) \rightarrow \infty$ with $m/n \rightarrow 0$. Then there exists a sequence of zero mean Gaussian random vectors $\{y_i\}_{i=1}^n$ that preserves the covariance structure of $\{z_i\}_{i=1}^n$, such that

$$(27) \quad \max_{a,b,a \leq b} \left\| \sum_{j=a}^b (Z_{j,m} - Y_{j,m}) \right\|_2 = O(d\sqrt{b-a+1}m^{1/s} \log m),$$

where $Y_{i,m} = \sum_{j=(i-1)m+1}^{im} y_i$, $i = 1, 2, \dots$ and s is defined in Theorem A.1.

Proof. The proof of this lemma follows the same martingale embedding and boundary conditioning arguments as those used in establishing [17, Theorem 3.1]. In

particular, Wasserstein Gaussian approximations are jointly applied to each block sum $Z_{i,m}$, $i = 1, 2, \dots$ to obtain

$$\max_i \|Z_{i,m} - Y_{i,m}\|_2 = O(dm^{1/s} \log m).$$

Then the lemma follows from the construction where the covariance between block sums $Z_{i,m} - Y_{i,m}$ for adjacent blocks are negligible. See [17, Theorem 3.1] for the details. \square

Theorem A.3. Under the same setup as that in Lemma A.2, we have that

$$\left\| \max_i \left| \sum_{j=1}^i (Z_{j,m} - Y_{j,m}) \right| \right\|_2 = O(d\sqrt{n/m}m^{1/s} \log_2(2n/m) \log m).$$

Proof. The proof of this Theorem is mainly based on the ‘‘bisection’’ technique in [1, page 102] with an induction argument. See also [22]. In particular, Theorem A.3 follows from similar proofs as those of [22, Theorems 3 and 4]. For the sake of completeness, we present the proof below.

Without loss of generality, assume that n is a multiple of m . Let $D_i = Z_{i,m} - Y_{i,m}$, $i = 1, 2, \dots, n/m$. Define $S_{l,k} = \sum_{j=l+1}^{l+k} D_j$ ($S_{l,0} = 0$) and $M_{l,k} = \max_{1 \leq j \leq k} |S_{l,j}|$, $l \geq 0$. By Lemma A.2, we have that

$$(28) \quad \max_l \|S_{l,k}\|_2 \leq Cd\sqrt{k}m^{1/s} \log m$$

for some finite constant $C > 0$, where $Y_{i,m} = \sum_{j=im-m+1}^{im} y_i$, $i = 1, 2, \dots$ and s is defined in Theorem A.1. We will use induction to show that

$$(29) \quad \|M_{l,k}\|_2 \leq C\sqrt{k} \log_2(2k)dm^{1/s} \log m \text{ for all } l \geq 0, k \geq 1.$$

The claim obviously holds for $k = 1$. Let m^* be the integer part of $n^*/2 + 1$ where $n^* = n/m$. Observe that if $m^* \leq k \leq n^*$, then

$$|S_{l,k}| \leq |S_{l,m^*}| + |S_{l+m^*,k-m^*}|.$$

As a result, we have $|S_{l,k}| \leq |S_{l,m^*}| + M_{l+m^*,n^*-m^*}$. On the other hand, $|S_{l,k}| \leq M_{l,m^*-1}$ if $k \leq m^* - 1$. Therefore, for $k \in [1, n^*]$, we have

$$|S_{l,k}| \leq |S_{l,m^*}| + [M_{l,m^*-1}^2 + M_{l+m^*,n^*-m^*}^2]^{1/2}.$$

Hence

$$|M_{l,n^*}| \leq |S_{l,m^*}| + [M_{l,m^*-1}^2 + M_{l+m^*,n^*-m^*}^2]^{1/2}.$$

By Minkowski's Inequality, we obtain that

$$(30) \quad \|M_{l,n^*}\|_2 \leq \|S_{l,m^*}\|_2 + [\|M_{l,m^*-1}\|_2^2 + \|M_{l+m^*,n^*-m^*}\|_2^2]^{1/2}.$$

Suppose that the conclusion in (29) holds for all integers $k < n^*$. We have by the induction hypothesis that $\|M_{l,m^*-1}\|_2 \leq C\sqrt{m^*-1} \log_2(2(m^*-1))dm^{1/s} \log m$ and $\|M_{l+m^*,n^*-m^*}\|_2 \leq C\sqrt{n^*-m^*} \log_2(2(n^*-m^*))dm^{1/s} \log m$. Simple calculations yield that

$$[\|M_{l,m^*-1}\|_2^2 + \|M_{l+m^*,n^*-m^*}\|_2^2]^{1/2} \leq C\sqrt{n^*} \log_2(2(m^*-1))dm^{1/s} \log m.$$

By (29), we have

$$\|S_{l,m^*}\|_2 \leq Cd\sqrt{m^*}m^{1/s} \log m \leq Cd\sqrt{n^*}m^{1/s} \log m.$$

Hence by (30), we have

$$\|M_{l,n^*}\|_2 \leq C\{\log_2(2(m^* - 1)) + 1\}\sqrt{n^*}dm^{1/s} \log m \leq C\log_2(2n^*)\sqrt{n^*}dm^{1/s} \log m.$$

The theorem follows by setting $l = 0$. \square

Proof of Theorem 3.1. Divide the sequence $\{z_i\}_{i=1}^n$ into blocks of size $L \leq n$, where L will be determined in the end, and denote $M := \lfloor n/L \rfloor$. The goal is applying Theorem A.1 to gain an approximation over each block, and control the Gaussian approximation using the weakly dependent structure of the blocks to obtain the final Gaussian approximation.

By Theorem A.1 and Theorem A.3, on a potentially richer probability space, we can find sequences of Gaussian random vectors $y_i \sim N(0, \text{cov}(z_i))$, and random vectors $\hat{z}_i \stackrel{\mathcal{D}}{=} z_i$, $i = 1, \dots, n$, such that

$$\begin{aligned} \mathbb{E} \left[\max_{r=1, \dots, M} \left| \frac{1}{\sqrt{n}} \sum_{k=1}^r Q_k \right|^2 \right] &= \frac{1}{n} \left\| \max_{r=1, \dots, M} \left\| \sum_{k=1}^r Q_k \right\|_2 \right\|^2 \\ (31) \qquad \qquad \qquad &= O(d^2 L^{2/s-1} \log_2^2(2n/L) \log^2(L)). \end{aligned}$$

where $Q_k := \sum_{j=(k-1)L+1}^{kL \wedge n} (\hat{z}_j - y_j)$ and s is defined in Theorem A.1.

By the Rosenthal inequality in Lemma A.1 and the fact that

$$\mathbb{E}[|y_i|^p] \leq C'(\mathbb{E}[|y_i|^2])^{p/2} = C'(\mathbb{E}[|\hat{z}_i|^2])^{p/2} \leq C' \mathbb{E}[|\hat{z}_i|^p]$$

for some constant C' depending only on p [21, Lemma 6.1], we have

$$(32) \quad \left(\mathbb{E} \left[\max_{r=(j-1)L+1, \dots, jL \wedge n} \left| \sum_{k=(j-1)L+1}^r \hat{z}_j \right|^p \right] \right)^{1/p} \leq C\sqrt{dL},$$

$$(33) \quad \left(\mathbb{E} \left[\max_{r=(j-1)L+1, \dots, jL \wedge n} \left| \sum_{k=(j-1)L+1}^r y_j \right|^p \right] \right)^{1/p} \leq CC'\sqrt{dL},$$

where $C = C_p [\Theta_p(1) + B^{1/p}]$ for some constant C_p that depends only on p .

Next, note that if $\max_{k=1, \dots, n} \left| \sum_{t=1}^k a_t \right|^2$ for a realization of random vectors $a_t := \hat{z}_t - y_t$, $t = 1, \dots, n$ is achieved at k^* , where $(j^* - 1)L + 1 \leq k^* < j^*L$, then

$$\left| \sum_{t=1}^{k^*} a_t \right|^2 = \left| \sum_{t=1}^{(j^*-1)L} a_t + \sum_{(j^*-1)L+1}^{k^*} a_t \right|^2 \leq 2 \left| \sum_{t=1}^{(j^*-1)L} a_t \right|^2 + 2 \left| \sum_{(j^*-1)L+1}^{k^*} a_t \right|^2.$$

Thus,

$$\max_{k=1, \dots, n} \left| \sum_{t=1}^k a_t \right|^2 \leq 2 \max_{r=1, \dots, M} \left| \sum_{t=1}^{(r-1)L} a_t \right|^2 + 2 \max_{1 \leq j \leq M} \max_{(j-1)L+1 \leq k \leq jL} \left| \sum_{(j-1)L+1}^k a_t \right|^2$$

and hence

$$\begin{aligned} & \left(\mathbb{E} \left[\max_{k=1, \dots, n} \left| \sum_{t=1}^k a_t \right|^2 \right] \right)^{1/2} \\ & \leq \sqrt{2} \left(\mathbb{E} \left[\max_{1 \leq r \leq M} \left| \sum_{t=1}^{(r-1)L} a_t \right|^2 \right] \right)^{1/2} + \sqrt{2} \left(\mathbb{E} \left[\max_{1 \leq r \leq M} \max_{(r-1)L+1 \leq k \leq rL} \left| \sum_{(r-1)L+1}^k a_t \right|^2 \right] \right)^{1/2}. \end{aligned}$$

Note that

$$\begin{aligned} & \left(\mathbb{E} \left[\max_{1 \leq r \leq M} \max_{(r-1)L+1 \leq k \leq rL} \left| \sum_{(r-1)L+1}^k a_t \right|^2 \right] \right)^{1/2} \\ & = \left(\mathbb{E} \left[\left(\max_{1 \leq r \leq M} \max_{(r-1)L+1 \leq k \leq rL} \left| \sum_{(r-1)L+1}^k a_t \right| \right)^2 \right] \right)^{1/2} \\ & = \left\| \max_{1 \leq r \leq M} \max_{(r-1)L+1 \leq k \leq rL} \left| \sum_{(r-1)L+1}^k a_t \right| \right\|_2 \\ & \leq \left\| \max_{1 \leq r \leq M} \max_{(r-1)L+1 \leq k \leq rL} \left| \sum_{(r-1)L+1}^k a_t \right| \right\|_p \\ & = \left(\mathbb{E} \left[\max_{1 \leq r \leq M} \max_{(r-1)L+1 \leq k \leq rL} \left| \sum_{(r-1)L+1}^k a_t \right|^p \right] \right)^{1/p}. \end{aligned}$$

Therefore,

$$\begin{aligned} (34) \quad & \left(\mathbb{E} \left[\max_{k=1, \dots, n} \left| \frac{1}{\sqrt{n}} \sum_{t=1}^k (\hat{z}_t - y_t) \right|^2 \right] \right)^{1/2} \\ & \leq \left(2 \mathbb{E} \left[\max_{r=1, \dots, M} \left| \frac{1}{\sqrt{n}} \sum_{k=1}^r Q_k \right|^2 \right] \right)^{1/2} \\ & \quad + \sqrt{2} \left(\mathbb{E} \left[\max_{1 \leq j \leq M} \max_{\substack{(j-1)L+1 \leq \\ k \leq jL}} \left| \frac{1}{\sqrt{n}} \sum_{t=(j-1)L+1}^{k \wedge n} (\hat{z}_t - y_t) \right|^p \right] \right)^{1/p} \\ & \leq \sqrt{2} \left(\mathbb{E} \left[\max_{r=1, \dots, M} \left| \frac{1}{\sqrt{n}} \sum_{k=1}^r Q_k \right|^2 \right] \right)^{1/2} \\ & \quad + \sqrt{2} M^{1/p} \max_{1 \leq j \leq M} \left(\mathbb{E} \left[\max_{\substack{(j-1)L+1 \leq k \\ \leq jL \wedge n}} \left| \frac{1}{\sqrt{n}} \sum_{t=(j-1)L+1}^{k \wedge n} (\hat{z}_t - y_t) \right|^p \right] \right)^{1/p}, \end{aligned}$$

where the second inequality comes from the bound

$$(\mathbb{E} \max_{1 \leq t \leq M} |\xi_t|^p)^{1/p} \leq M^{1/p} \max_{1 \leq t \leq M} (\mathbb{E}[|\xi_t|^p])^{1/p}$$

for any random variables ξ_1, \dots, ξ_M . The first term in the right hand side of (34) can be bounded by (31) and the second term can be bounded by (32). As a result, (34) is controlled by

$$(35) \quad \left(\mathbb{E} \left[\max_{k=1, \dots, n} \left| \frac{1}{\sqrt{n}} \sum_{t=1}^k (\hat{z}_t - y_t) \right|^2 \right] \right)^{1/2} \\ \leq C_1 d L^{1/s-1/2} \log_2 \left(\frac{2n}{L} \right) \log(L) + \sqrt{2} C(C' + 1) M^{1/p} \sqrt{\frac{Ld}{n}} \\ \leq C_1 d \left(\frac{n}{M} \right)^{1/s-1/2} \log_2(2M) \log \left(\frac{n}{M} \right) + \sqrt{2} C(C' + 1) M^{1/p-1/2} \sqrt{d}$$

for some $C_1 > 0$. By choosing L so that the right hand side is balanced, we have $M = \left(\frac{n^{1/2-1/s}}{d^{1/2}} \right)^{1-1/s-1/p}$, and hence

$$\left(\mathbb{E} \left[\max_{k=1, \dots, n} \left| \frac{1}{\sqrt{n}} \sum_{t=1}^k (\hat{z}_t - y_t) \right|^2 \right] \right)^{1/2} = O \left(\left(\frac{d^{\frac{3}{4}-\frac{1}{2s}-\frac{1}{p}}}{n^{\frac{1}{4}-\frac{1}{2p}-\frac{1}{2s}+\frac{1}{ps}}} \right)^{1-\frac{1}{s}-\frac{1}{p}} \log(n)^2 \right),$$

where the implied constant depends on p and the dependence structure and moment control of z_i . \square

A.2. Proof of Lemma 3.1.

Proof. The p -norm bound of Assumptions 2.2 is immediate by the boundedness of sine and cosine functions. Next, note that \mathbf{X}_j is generated by $\mathbf{X}_j = \tilde{\mathcal{G}}_i(\mathcal{F}_i)$, where

$$\tilde{\mathcal{G}}_i : \mathbb{R}^\infty \rightarrow \mathbb{R}^{2d} \text{ via } \tilde{\mathcal{G}}_i(\mathcal{F}_i) := \begin{bmatrix} \mathcal{G}(\mathcal{F}_i) \cos(2\pi\eta_1 j) \\ \vdots \\ \mathcal{G}(\mathcal{F}_i) \sin(2\pi\eta_d j) \end{bmatrix}. \text{ Thus, the polynomial decay of}$$

the dependence measure of \mathbf{X}_j in Assumption 2.2 holds based on the assumption of X_i . Finally, the moment bound holds since cos and sin functions are bounded by 1. \square

A.3. Proof of Theorem 3.2: the Gaussianity of STFT.

Proof. Denote $\alpha_t \in \mathbb{C}^{2d \times 4d}$ so that $\alpha_t(k, k+2d) = e^{i2\pi\eta_k t}$ and $\alpha_t(k+d, k+3d) = ie^{i2\pi\eta_k t}$ for $k = 1, \dots, d$ and 0 otherwise. Consider $\mathbf{X}_j \in \mathbb{R}^{2d}$ in Lemma 3.1. Denote the partial sum

$$\mathbf{S}_j = \sum_{l=1}^j \mathbf{X}_l \in \mathbb{R}^{2d}$$

with $\mathbf{S}_j = 0$ when $j \leq 0$. We then have

$$\begin{aligned} \mathbf{V}_t &= \alpha_t \left[\begin{array}{l} \sum_{j=t-m}^{t+m} \mathbf{X}_j \mathbf{h}(j-t) \\ \sum_{j=t-m}^{t+m} \mathbf{X}_j \mathbf{Dh}(j-t) \end{array} \right] \\ &= \alpha_t \left[\begin{array}{l} \sum_{j=t-m}^{t+m} (\mathbf{S}_j - \mathbf{S}_{j-1}) \mathbf{h}(j-t) \\ \sum_{j=t-m}^{t+m} (\mathbf{S}_j - \mathbf{S}_{j-1}) \mathbf{Dh}(j-t) \end{array} \right] \\ &= \alpha_t \left[\begin{array}{l} \sum_{j=t-m}^{t+m} \mathbf{S}_j (\mathbf{h}(j-t) - \mathbf{h}(j-1-t)) - \mathbf{S}_{t-m-1} \mathbf{h}(-m) \\ \sum_{j=t-m}^{t+m} \mathbf{S}_j (\mathbf{Dh}(j-t) - \mathbf{Dh}(j-1-t)) - \mathbf{S}_{t-m-1} \mathbf{Dh}(-m) \end{array} \right] \end{aligned}$$

Suppose $\{Z_i\}_{i \in \mathbb{Z}}$ is the Gaussian approximation of X_i on a potentially richer probability space, $\hat{\mathbf{S}}_j$ is the associated partial sum, and $\hat{\mathbf{V}}_t \in \mathbb{C}^{2d}$ is the associated complex Gaussian random vector defined like \mathbf{V}_t . We have

$$\begin{aligned} &\mathbf{V}_t - \hat{\mathbf{V}}_t \\ &= \alpha_t \left[\begin{array}{l} \sum_{j=t-m}^{t+m} (\mathbf{S}_j - \hat{\mathbf{S}}_j) (\mathbf{h}(j-t) - \mathbf{h}(j-1-t)) - (\mathbf{S}_{t-m-1} - \hat{\mathbf{S}}_{t-m-1}) \mathbf{h}(-m) \\ \sum_{j=t-m}^{t+m} (\mathbf{S}_j - \hat{\mathbf{S}}_j) (\mathbf{Dh}(j-t) - \mathbf{Dh}(j-1-t)) - (\mathbf{S}_{t-m-1} - \hat{\mathbf{S}}_{t-m-1}) \mathbf{Dh}(-m) \end{array} \right]. \end{aligned}$$

A direct bound leads to

$$\begin{aligned} &\left| \frac{1}{\sqrt{n}} (\mathbf{V}_t - \hat{\mathbf{V}}_t) \right|^2 \\ &\leq 2 \sum_{j=t-m}^{t+m} \left| \frac{1}{\sqrt{n}} (\mathbf{S}_j - \hat{\mathbf{S}}_j) \right|^2 (|\mathbf{h}(j-t) - \mathbf{h}(j-1-t)|^2 + |\mathbf{Dh}(j-t) - \mathbf{Dh}(j-1-t)|^2) \\ &\quad + 2 \left| \frac{1}{\sqrt{n}} (\mathbf{S}_{t-m-1} - \hat{\mathbf{S}}_{t-m-1}) \right|^2 (\mathbf{h}(-m)^2 + \mathbf{Dh}(-m)^2) \\ &= 2 \sum_{j=t-m}^{t+m} \left| \frac{1}{\sqrt{n}} (\mathbf{S}_j - \hat{\mathbf{S}}_j) \right|^2 (|\mathbf{h}(j-t) - \mathbf{h}(j-1-t)|^2 + |\mathbf{Dh}(j-t) - \mathbf{Dh}(j-1-t)|^2), \end{aligned}$$

where the last equality holds since \mathbf{h} is assumed to be supported on $[-1/2, 1/2]$. We then control $\frac{1}{\sqrt{n}} (\mathbf{S}_j - \hat{\mathbf{S}}_j)$ by $\max_{t=1, \dots, n} \left| \frac{1}{\sqrt{n}} (\mathbf{S}_t - \hat{\mathbf{S}}_t) \right|^2$ using Theorem 3.1. Note that $\mathbf{X}_i \in \mathbb{R}^{2d}$ fulfills the necessary assumptions by Lemma 3.1. As a result, we obtain

$$\left[\mathbb{E} \left(\max_{t=1, \dots, n} \left| \frac{1}{\sqrt{n}} (\mathbf{S}_t - \hat{\mathbf{S}}_t) \right|^2 \right) \right]^{1/2} \leq C \left(\frac{d^{\frac{3}{4} - \frac{1}{2s} - \frac{1}{p}}}{n^{\frac{1}{4} - \frac{1}{2p} - \frac{1}{2s} + \frac{1}{ps}}} \right)^{\frac{1}{1 - \frac{1}{s} - \frac{1}{p}}} \log(n)^2,$$

where $C > 0$ is a constant depending on p and the dependence structure and moment control of X_i . On the other hand, by the definition of $\mathbf{h}(j-t)$, we have

$$\begin{aligned} &\max_{t=1, \dots, n} \sum_{j=t-m}^{t+m} (|\mathbf{h}(j-t) - \mathbf{h}(j-1-t)|^2 + |\mathbf{Dh}(j-t) - \mathbf{Dh}(j-1-t)|^2) \\ &= \max_t \frac{1}{m} \sum_{j=t-m}^{t+m} \left(\left| \mathbf{h} \left(\frac{j-t}{2m+1} \right) - \mathbf{h} \left(\frac{j-t-1}{2m+1} \right) \right|^2 + \left| \mathbf{h}' \left(\frac{j-t}{2m+1} \right) - \mathbf{h}' \left(\frac{j-t-1}{2m+1} \right) \right|^2 \right) \\ &= \Theta(m^{-2}), \end{aligned}$$

where the implied constant depends on $\|\mathbf{h}'\|_2$, $\|\mathbf{h}''\|_2$, $\|\mathbf{h}''\|_\infty$ and $\|\mathbf{h}'''\|_\infty$ since $m \left(\mathbf{h} \left(\frac{j-t}{2m+1} \right) - \mathbf{h} \left(\frac{j-t-1}{2m+1} \right) \right)$ is a finite difference approximation of $\mathbf{h}' \left(\frac{j-t-1}{2m+1} \right)$ and $\frac{1}{m} \sum_{j=t-m}^{t+m} \left| \mathbf{h}' \left(\frac{j-t}{2m+1} \right) \right|^2$ is a Riemann sum approximation of $\|\mathbf{h}'\|_2$. By putting the above together, we have the claim by

$$\begin{aligned}
& \mathbb{E} \left(\max_t \left| \frac{1}{\sqrt{n}} (\mathbf{V}_t - \hat{\mathbf{V}}_t) \right|^2 \right) \\
& \leq \mathbb{E} \left(\max_t \sum_{j=t-m}^{t+m} \max_{j \leq n} \left| \frac{1}{\sqrt{n}} (\mathbf{S}_j - \hat{\mathbf{S}}_j) \right|^2 \right. \\
& \quad \left. \times (|\mathbf{h}(j-t) - \mathbf{h}(j-1-t)|^2 + |\mathbf{Dh}(j-t) - \mathbf{Dh}(j-1-t)|^2) \right) \\
& \leq \mathbb{E} \left(\max_{j \leq n} \left| \frac{1}{\sqrt{n}} (\mathbf{S}_j - \hat{\mathbf{S}}_j) \right|^2 \right) \\
& \quad \times \max_t \sum_{j=t-m}^{t+m} (|\mathbf{h}(j-t) - \mathbf{h}(j-1-t)|^2 + |\mathbf{Dh}(j-t) - \mathbf{Dh}(j-1-t)|^2) \\
& \leq C' \left(\frac{d^{\frac{3}{4} - \frac{1}{2s} - \frac{1}{p}}}{n^{\frac{1}{4} - \frac{1}{2p} - \frac{1}{2s} + \frac{1}{ps}}} \right)^{\frac{2}{1 - \frac{1}{s} - \frac{1}{p}}} \log(n)^4 m^{-2},
\end{aligned}$$

where $C' > 0$ is a constant depending on \mathbf{h} and the moment and dependence structures of ϵ_i . \square

A.4. Proof of Theorem 4.2: robustness of SST-based reconstruction formula. We require the following lemma concerning the magnitude of the discrete STFT of noise. This lemma is an immediate consequence of Theorem 3.2. This result may be of independent interest.

Lemma A.2. Suppose $\{\epsilon_i\}_{i=1}^n$ satisfies the NSN model and Assumption 2.2, with the condition $A > \sqrt{\chi} + 1$ fulfilled. Suppose $d = n^{1/3-\gamma}$ for a small $\gamma \in (0, 1/3)$ and consider $0 < \eta_1 < \dots < \eta_d$. Denote a complex random vector associated with the discrete STFT (1):

$$\mathbf{V}_l := [\mathbf{V}_\epsilon^{(\mathbf{h})}(l, \eta_1), \dots, \mathbf{V}_\epsilon^{(\mathbf{h})}(l, \eta_d), \mathbf{V}_\epsilon^{(\mathbf{Dh})}(l, \eta_1), \dots, \mathbf{V}_\epsilon^{(\mathbf{Dh})}(l, \eta_d)]^\top \in \mathbb{C}^{2d},$$

where \mathbf{h} and \mathbf{Dh} are defined in (4) and (8) with $m := \lceil \beta \sqrt{n} \rceil$. Then we have

$$\max_l |\mathbf{V}_l| = o_p(\sqrt{d \log d}),$$

and

$$\max_l |\mathbf{V}_l|_\infty \leq C' \sqrt{\log d}$$

with probability higher than $1 - d^{-3}$.

Proof. By Theorem 3.2, we know that $\mathbf{V}_\epsilon^{(\mathbf{h})}(l, \eta_k)$ is approximately Gaussian in the following sense. Denote

$$\hat{\mathbf{V}}_l := [\mathbf{V}_\epsilon^{(\mathbf{h})}(l, \eta_1), \dots, \mathbf{V}_\epsilon^{(\mathbf{h})}(l, \eta_d), \mathbf{V}_\epsilon^{(\mathbf{Dh})}(l, \eta_1), \dots, \mathbf{V}_\epsilon^{(\mathbf{Dh})}(l, \eta_d)]^\top \in \mathbb{C}^{2d},$$

where $\hat{\epsilon}$ is the Gaussian approximation of ϵ stated in Theorem 3.2. Then, we have

$$\mathbb{E} \left(\max_l \left| \frac{1}{\sqrt{n}} (\mathbf{V}_l - \hat{\mathbf{V}}_l) \right|^2 \right) \leq C' d \left(\frac{d^{1/2}}{n^{1/2-1/s}} \right)^{\frac{1-2/p}{3/2-1/s-1/p}} (\log n)^2 m^{-2},$$

where C' is a universal constant. Since

$$|\mathbf{V}_\epsilon^{(\mathbf{h})}(l, \eta_k)| \leq |\mathbf{V}_{\hat{\epsilon}}^{(\mathbf{h})}(l, \eta_k)| + |\mathbf{V}_\epsilon^{(\mathbf{h})}(l, \eta_k) - \mathbf{V}_{\hat{\epsilon}}^{(\mathbf{h})}(l, \eta_k)|$$

and a similar bound holds when the superscript \mathbf{h} is replaced by \mathbf{h}' , we have

$$\max_l |\mathbf{V}_l| \leq \max_l |\hat{\mathbf{V}}_l| + \max_l |\mathbf{V}_l - \hat{\mathbf{V}}_l|.$$

By the Chebychev inequality, we have

$$\max_l \left| \frac{1}{\sqrt{n}} (\mathbf{V}_l - \hat{\mathbf{V}}_l) \right| = o_p \left(\left(\frac{d^{\frac{3}{4} - \frac{1}{2s} - \frac{1}{p}}}{n^{\frac{1}{4} - \frac{1}{2p} - \frac{1}{2s} + \frac{1}{ps}}} \right)^{\frac{1}{1 - \frac{1}{s} - \frac{1}{p}}} \frac{\log(n)}{m} \right).$$

On the other hand, since $\hat{\mathbf{V}}_l$ is a non-degenerate $2d$ -dim complex Gaussian random vector whose entrywise variance is of order 1, we have

$$|\hat{\mathbf{V}}_l|_\infty \leq C \sqrt{\log d},$$

and hence

$$|\hat{\mathbf{V}}_l| \leq C \sqrt{d \log d},$$

with probability higher than $1 - d^{-3}$. By a union bound, $\max_l \left| \frac{1}{\sqrt{n}} \hat{\mathbf{V}}_l \right|^2$ can be bounded by $\frac{Cd \log d}{n}$ for some constant $C > 0$ with probability higher than $1 - nd^{-3}$. Therefore, we have

$$\max_l |\mathbf{V}_l| = o_p \left(\left(\frac{d^{\frac{3}{4} - \frac{1}{2s} - \frac{1}{p}}}{n^{\frac{1}{4} - \frac{1}{2p} - \frac{1}{2s} + \frac{1}{ps}}} \right)^{\frac{1}{1 - \frac{1}{s} - \frac{1}{p}}} \frac{(\log n)^2 \sqrt{n}}{m} + \sqrt{d \log d} \right).$$

To obtain the uniform bound, note that by construction, $\hat{\mathbf{V}}_l$ and \mathbf{V}_l share the same covariance matrix. Thus, \mathbf{V}_l a non-degenerate $2d$ -dim complex random vector whose entrywise variance is of order 1, by the same argument used in [34] following the technique for maxima control [4, 5], we obtain

$$\max_l |\mathbf{V}_l|_\infty \leq C' \sqrt{\log d}$$

with probability higher than $1 - d^{-3}$, where $C' > 0$ depends on the moment and dependence structure of ϵ_i . □

The following result is about how STFT behaves on an oscillatory signal satisfying AHM in the discretized setup (3). We precisely describe its behavior and the associated numerical approximation error.

Lemma A.3. Suppose $\{f_i\}_{i=1}^n$ in model (11) satisfies $f_i = f(t_i)$, where f satisfies the AHM with Assumption (2.1) fulfilled and $t_i = i/\sqrt{n}$. Denote $\mathbf{f} := [f(t_1), \dots, f(t_n)]^\top \in \mathbb{R}^n$. Assume Assumption (4.1) holds. Denote $J_k^{(m)} := \int_{-\infty}^{\infty} |u|^k |\mathbf{h}^{(m)}(u)| du$, the $k \in \mathbb{N} \cup \{0\}$ th absolute moment of the m -th derivative of \mathbf{h} . Then, for any $\eta \in (0, \sqrt{n}/2)$,

$$(36) \quad E_{f,l,\eta} := V_{\mathbf{f}}^{(\mathbf{h})}(t_l, \eta) - A(t_l) e^{i2\pi\phi(t_l)} \hat{\mathbf{h}}(\eta - \phi'(t_l)),$$

satisfies

$$E_f := \max_l \sup_{\eta \in (0, \Xi)} |E_{f,l,\eta}| \leq \varepsilon \Xi_A (J_1^{(0)} + \pi \Xi J_2^{(0)}) + \frac{\Xi_A ((\varepsilon + \Xi) \|\mathbf{h}\|_\infty + \|\mathbf{h}'\|_\infty) \beta}{\sqrt{n}},$$

and

$$(37) \quad E'_{f,l,\eta} := \frac{1}{2\pi i} V_{\mathbf{f}}^{(h')} (t_l, \eta) - (\eta - \phi'(t_l)) A(t_l) \widehat{\mathbf{h}}(\eta - \phi'(t_l)) e^{i2\pi\phi(t)}$$

satisfies

$$\begin{aligned} E'_f &:= \max_l \sup_{\eta \in (0, \Xi)} |E'_{f,l,\eta}| \\ &\leq \varepsilon \Xi_A \left(\frac{J_0^{(0)}}{2\pi} + 2\Xi J_1^{(0)} + \pi \Xi^2 J_2^{(0)} \right) + \frac{\Xi_A ((\varepsilon + \Xi) \|\mathbf{h}'\|_\infty + \|\mathbf{h}''\|_\infty) \beta}{\sqrt{n}}. \end{aligned}$$

The reassignment rule satisfies that when $|V_{\mathbf{f}}^{(h)}(t_l, \eta)| > \tau$ for some $\tau \geq 0$, we have

$$(38) \quad E_{O,l,\eta} := O_{\mathbf{f}}^{(\tau)}(t_l, \eta) - \phi'(t_l)$$

satisfies

$$E_O^{(\tau)} := \max_l \max_{\substack{\eta \in (0, \Xi) \\ |V_{\mathbf{f}}^{(h)}(t_l, \eta)| > \tau}} |E_{O,l,\eta}| \leq \frac{E'_f + \Xi E_f}{\tau}.$$

Set $B_l := [\phi'(t_l) - \Delta, \phi'(t_l) + \Delta]$. Then, we have

$$(39) \quad E_{r,l} := \frac{1}{h(0)} \frac{\Xi}{d} \sum_{k \in B_l} V_{\mathbf{f}}^{(h)}(t_l, \eta_k) - A(t_l) e^{i2\pi\phi(t_l)}$$

satisfying

$$\begin{aligned} E_r := \max_l |E_{r,l}| &\leq \frac{\pi^2 \Xi^2 \Xi_A \Delta}{3d^2 h(0)} \left((1 + \varepsilon \beta) J_2^{(0)} + \frac{4\beta((\varepsilon \|\mathbf{h}\|_\infty + \|\mathbf{h}'\|_\infty) \beta + \|\mathbf{h}\|_\infty)}{\sqrt{n}} \right) \\ &\quad + \frac{2(E_f \Delta + \Xi_A \beta^{-1/2} \delta_2)}{h(0)}, \end{aligned}$$

where $\frac{\Xi}{d} \sum_{k \in B_l} V_{\mathbf{f}}^{(h)}(t_l, \eta_k)$ is the reconstruction formula associated with the discretized STFT.

Remark. In this lemma, we explicitly identify each error term, as each one plays a distinct role in establishing the uniform error bound required later. For instance, consider (39). Since $d = d(n) \rightarrow \infty$ as $n \rightarrow \infty$, when $n \rightarrow \infty$, the reconstruction error asymptotically approaches $\frac{2(E_f \Delta + \Xi_A \beta^{-1/2} \delta)}{h(0)}$. Moreover, when the signal is harmonic; that is, when $\varepsilon = 0$, this error simplifies to $\frac{2\Xi_A \beta^{-1/2} \delta}{h(0)}$, which corresponds to the spectral truncation in the reconstruction formula. Notably, all error terms scale with Ξ_A , highlighting that the reconstruction error scales properly according to the signal's amplitude.

Proof. The behavior of $V_{\mathbf{f}}^{(h)}(t_1, \eta)$ and $V_{\mathbf{f}}^{(h')} (t_1, \eta)$ is well known in the literature. See, for example, [32]. It is worth noting that in the main result of interest, [32, Theorem 2.3.14], the control over $|A'(t)|$ differs from ours. Here, we choose to emphasize the role of $A(t)$ directly, as it allows us to achieve a clearer and more uniform bound in the final result.

The study of $V_{\mathbf{f}}^{(\mathbf{h})}(t_l, \eta)$ and $V_{\mathbf{f}}^{(\mathbf{Dh})}(t_l, \eta)$ is via viewing them as Riemann sums and studying the numerical approximation error. Note that there are $\lfloor 2\beta/\sqrt{n} \rfloor$ sampled points over $[-\beta, \beta]$ since \mathbf{h} is supported on $[-\beta, \beta]$. Also, we have $\|(f\mathbf{h})'\|_{\infty} \leq \|A'\|_{\infty}\|\mathbf{h}\|_{\infty} + \|A\|_{\infty}\|\phi'\|_{\infty}\|\mathbf{h}\|_{\infty} + \|A\|_{\infty}\|\mathbf{h}'\|_{\infty} \leq \Xi_A((\varepsilon + \Xi)\|\mathbf{h}\|_{\infty} + \|\mathbf{h}'\|_{\infty})$. By the Riemann sum error approximation, we have

$$(40) \quad \begin{aligned} & \left| V_{\mathbf{f}}^{(\mathbf{h})}(t_l, \eta) - V_f^{(\mathbf{h})}(t_l, \eta) \right| \\ &= \left| \frac{1}{\sqrt{n}} \sum_{j=1}^n f(t_j) \mathbf{h}(t_j - t_l) e^{-i2\pi\eta(t_j - t_l)} - V_f^{(\mathbf{h})}(t_l, \eta) \right| \\ &\leq \frac{\Xi_A((\varepsilon + \Xi)\|\mathbf{h}\|_{\infty} + \|\mathbf{h}'\|_{\infty})\beta}{\sqrt{n}}, \end{aligned}$$

and hence the claimed bound

$$\begin{aligned} & \left| V_{\mathbf{f}}^{(\mathbf{h})}(t_l, \eta) - A(t_l) \widehat{\mathbf{h}}(\eta - \phi'(t_l)) e^{i2\pi\phi(t_l)} \right| \\ &\leq \varepsilon \Xi_A(J_1^{(0)} + \pi \Xi J_2^{(0)}) + \frac{\Xi_A((\varepsilon + \Xi)\|\mathbf{h}\|_{\infty} + \|\mathbf{h}'\|_{\infty})\beta}{\sqrt{n}} =: E_f, \end{aligned}$$

where the bound comes from [32, Theorem 2.3.14]. Note that in [32, Theorem 2.3.14], the control of $|A'(t)|$ is different from what we consider here. Similarly, we have

$$\left| \frac{1}{2\pi i} V_{\mathbf{f}}^{(\mathbf{h}')} (t_l, \eta) - \frac{1}{2\pi i} V_f^{(\mathbf{h}')} (t_l, \eta) \right| \leq \frac{\Xi_A((\varepsilon + \Xi)\|\mathbf{h}'\|_{\infty} + \|\mathbf{h}''\|_{\infty})\beta}{\sqrt{n}}$$

and hence with [32, Theorem 2.3.14], we obtain

$$\begin{aligned} & \left| \frac{1}{2\pi i} V_{\mathbf{f}}^{(\mathbf{h}')} (t_l, \eta) - (\eta - \phi'(t_l)) A(t_l) \widehat{\mathbf{h}}(\eta - \phi'(t_l)) e^{i2\pi\phi(t_l)} \right| \\ &\leq \varepsilon \Xi_A \left(\frac{J_0^{(0)}}{2\pi} + 2\Xi J_1^{(0)} + \pi \Xi^2 J_2^{(0)} \right) + \frac{\Xi_A((\varepsilon + \Xi)\|\mathbf{h}\|_{\infty} + \|\mathbf{h}'\|_{\infty})\beta}{\sqrt{n}} =: E'_f. \end{aligned}$$

For the reassignment rule, note that by the above Riemann sum approximation, when n is sufficiently large, we have when $|V_{\mathbf{f}}^{(\mathbf{h})}(t_l, \eta)| > \tau$ for $\tau > 0$, where $\eta \in (0, \Xi)$,

$$\begin{aligned} |O_{\mathbf{f}}^{(\tau)}(t_l, \eta) - \phi'(t_l)| &= \left| \frac{-1}{2\pi i} \frac{V_{\mathbf{f}}^{(\mathbf{h}')} (t_l, \eta)}{V_{\mathbf{f}}^{(\mathbf{h})} (t_l, \eta)} - \phi'(t_l) \right| \\ &= \left| \frac{-A(t_l) \phi'(t_l) e^{i2\pi\phi(t_l)} \widehat{\mathbf{h}}(\eta - \phi'(t_l)) - E'_{f,l,k}}{V_{\mathbf{f}}^{(\mathbf{h})} (t_l, \eta)} - \phi'(t_l) \right| \\ &\leq \frac{E'_f + \phi'(t_l) E_f}{|V_{\mathbf{f}}^{(\mathbf{h})} (t_l, \eta)|} \leq \frac{E'_f + \Xi E_f}{|V_{\mathbf{f}}^{(\mathbf{h})} (t_l, \eta)|} \end{aligned}$$

and hence the claim.

For the final claim about the discretized STFT reconstruction formula, rewrite

$$\frac{\Xi}{d} \sum_{k \in B_l} V_{\mathbf{f}}^{(\mathbf{h})}(t_l, \eta_k) = \frac{1}{\sqrt{n}} \sum_{j=1}^n f(t_j) \mathbf{h}(t_j - t_l) \left[\frac{\Xi}{d} \sum_{k \in B_l} e^{-i2\pi\eta_k(t_j - t_l)} \right].$$

By the Riemann sum approximation, we obtain

$$\left| \frac{\Xi}{d} \sum_{k \in B_l} e^{-i2\pi\eta_k(t_j - t_l)} - \int_{B_l} e^{-i2\pi\eta(t_j - t_l)} d\eta \right| \leq \frac{\pi^2 \Xi^2 \Delta}{3d^2} (t_j - t_l)^2.$$

Therefore, since $|f(t)| \leq A(t)$ and \mathbf{h} is nonnegative by assumption,

$$(41) \quad \left| \frac{\Xi}{d} \sum_{k \in B_l} V_{\mathbf{f}}^{(\mathbf{h})}(t_l, \eta_k) - \int_{B_l} V_{\mathbf{f}}^{(\mathbf{h})}(t_l, \eta) d\eta \right| \\ \leq \frac{\pi^2 \Xi^2 \Delta}{3d^2} \frac{1}{\sqrt{n}} \sum_{j=1}^n A(t_j) \mathbf{h}(t_j - t_l) (t_j - t_l)^2 \\ \leq \frac{\pi^2 \Xi^2 \Xi_A \Delta}{3d^2} \left((1 + \varepsilon\beta) J_2^{(0)} + \frac{4\beta((\varepsilon\|\mathbf{h}\|_\infty + \|\mathbf{h}'\|_\infty)\beta + \|\mathbf{h}\|_\infty)}{\sqrt{n}} \right),$$

where the last bound comes from the Riemann sum approximation

$$\left| \frac{1}{\sqrt{n}} \sum_{j=1}^n A(t_j) \mathbf{h}(t_j - t_l) (t_j - t_l)^2 I(|t_j - t_l| \leq \beta) - \int_{-\beta}^{\beta} A(t + t_l) \mathbf{h}(t) t^2 dt \right| \\ \leq \frac{4\Xi_A \beta((\varepsilon\|\mathbf{h}\|_\infty + \|\mathbf{h}'\|_\infty)\beta + \|\mathbf{h}\|_\infty)}{\sqrt{n}}$$

and the approximation that

$$\left| \int_{-\beta}^{\beta} A(t + t_l) \mathbf{h}(t) t^2 dt - A(t_l) J_2^{(0)} \right| \leq \varepsilon\beta \Xi_A J_2^{(0)}.$$

Moreover,

$$(42) \quad \left| \frac{1}{\mathbf{h}(0)} \int_{B_l} V_{\mathbf{f}}^{(\mathbf{h})}(t_l, \eta) d\eta - A(t_l) e^{i2\pi\phi(t_l)} \right| \\ = \frac{1}{\mathbf{h}(0)} \left| \int_{B_l} V_{\mathbf{f}}^{(\mathbf{h})}(t_l, \eta) d\eta - \int_{-\infty}^{\infty} A(t_l) e^{i2\pi\phi(t_l)} \widehat{\mathbf{h}}(\eta - \phi'(t_l)) d\eta \right| \\ \leq \frac{1}{\mathbf{h}(0)} \left| \int_{B_l} \left[V_{\mathbf{f}}^{(\mathbf{h})}(t_l, \eta) - A(t_l) e^{i2\pi\phi(t_l)} \widehat{\mathbf{h}}(\eta - \phi'(t_l)) \right] d\eta \right| \\ + \frac{1}{\mathbf{h}(0)} \left| \int_{\mathbb{R} \setminus B_l} A(t_l) e^{i2\pi\phi(t_l)} \widehat{\mathbf{h}}(\eta - \phi'(t_l)) d\eta \right| \\ \leq \frac{2E_f \Delta}{\mathbf{h}(0)} + \frac{\Xi_A}{\mathbf{h}(0)} \int_{\mathbb{R} \setminus B_l} |\widehat{\mathbf{h}}(\eta - \phi'(t_l))| d\eta \leq \frac{2E_f \Delta + \Xi_A \beta^{-1/2} \delta_2}{\mathbf{h}(0)}.$$

By putting (41) and (42) together, when n is sufficiently large, we obtain

$$\left| \frac{1}{\mathbf{h}(0)} \frac{\Xi}{d} \sum_{k \in B_l} V_{\mathbf{f}}^{(\mathbf{h})}(t_l, \eta_k) - A(t_l) e^{i2\pi\phi(t_l)} \right| \\ \leq \frac{\pi^2 \Xi^2 \Xi_A \Delta}{3d^2 \mathbf{h}(0)} \left((1 + \varepsilon\beta) J_2^{(0)} + \frac{4\beta((\varepsilon\|\mathbf{h}\|_\infty + \|\mathbf{h}'\|_\infty)\beta + \|\mathbf{h}\|_\infty)}{\sqrt{n}} \right) + \frac{2(E_f \Delta + \Xi_A \beta^{-1/2} \delta)}{\mathbf{h}(0)},$$

and hence the claimed bound. \square

Corollary A.4. Grant the same notation and assumptions in Lemma A.3. Set $B_l := [\phi'(t_l) - \Delta, \phi'(t_l) + \Delta]$. Then, when n is sufficiently large, we have

$$(43) \quad \min_l \min_{\eta \in B_l} |V_{\mathbf{f}}^{(h)}(t_l, \eta)| \geq \Xi_a \sqrt{\beta} \delta_1 / 2 =: \nu_0$$

for some constant $C'_h > 2$ depending on h .

Proof. The proof is an immediate consequence of Lemma A.3. Since for any $l = 1, \dots, n$, by the assumption of h , when $\eta \in B_l$, we have

$$|V_{\mathbf{f}}^{(h)}(t_l, \eta)| \geq A(t_l) |\widehat{h}(\eta - \phi'(t_l))| - 2\varepsilon \Xi_A (J_1^{(0)} + \pi \Xi J_2^{(0)}) \geq \Xi_a \sqrt{\beta} \delta_1 / 2. \quad \square$$

The following lemma prepares a control of a key quantity that we need when we analyze the SST reconstruction formula. We start with a clean case, which will serve as the base for the noisy case.

Lemma A.4. Suppose $f_i = f(t_i)$, f satisfies the AHM with $\varepsilon > 0$ and Assumption (2.1) fulfilled, $t_i = i/\sqrt{n}$. Set $m = \lceil \beta \sqrt{n} \rceil$ and $d = d(n) \rightarrow \infty$ when $n \rightarrow \infty$. Set $\eta_k = \frac{k\Xi}{d}$, where $k = 1, \dots, d$. Grant the kernel assumption in Assumption 4.1 and choose Δ so that $\frac{2(E'_f + \Xi E_f)}{\Xi_a \sqrt{\beta} \delta_1} \leq 1/2$. For $l \in \{1, \dots, n\}$, denote

$$(44) \quad \begin{aligned} R_l &:= [\phi'(t_l) - \Delta_r, \phi'(t_l) + \Delta_r] \\ B_l &:= [\phi'(t_l) - \Delta, \phi'(t_l) + \Delta] \\ Q_l &:= \{\eta \in (0, \Xi) \mid |V_{\mathbf{f}}^{(h)}(t_l, \eta)| > \nu_0\}. \end{aligned}$$

We have $B_l \subset Q_l$. Set

$$(45) \quad \nu_0 = \Xi_a \sqrt{\beta} \delta_1 / 2 \quad \text{and} \quad \alpha = \left(\frac{\Delta_r}{2C_\alpha} \right)^2$$

for some $C_\alpha > 1$. Then, when n is sufficiently large, we have

$$(46) \quad E_{g,l,k} := \frac{\Xi}{d} \sum_{\eta_j \in R_l} g_\alpha(\eta_j - O_{\mathbf{f}}^{(\nu_0)}(t_l, \eta_k)) - 1,$$

satisfying

$$E_g := \max_l \max_{\eta_k \in Q_l} |E_{g,l,k}| \leq 2 \operatorname{erfc}(C_\alpha) + \frac{\Xi C_\alpha^3}{\sqrt{\pi} \Delta_r^3 d}.$$

When $\eta_k \notin Q_l$, we have

$$\frac{\Xi}{d} \sum_{\eta_j \in R_l} g_\alpha(\eta_j - O_{\mathbf{f}}^{(\nu_0)}(t_l, \eta_k)) = 0.$$

Remark. Note that there are two dominant terms controlling E_g . The first term is regarding the truncation of integration in the frequency domain, and the second term is regarding the discretization of the frequency domain.

Proof. Since η_j is a uniform discretization in the frequency axis, we approximate $\frac{\Xi}{d} \sum_{\eta_j \in R_l} g_\alpha(\eta_j - O_{\mathbf{f}}^{(\nu_0)}(t_l, \eta_k))$ by $\int_{R_l} g_\alpha(\eta - O_{\mathbf{f}}^{(\nu_0)}(t_l, \eta_k)) d\eta$. By the Riemann sum

approximation, when $|V_{\mathbf{f}}^{(h)}(t_l, \eta)| > \nu_0$, we have

$$\left| \frac{\Xi}{d} \sum_{\eta_j \in R_l} g_\alpha(\eta_j - O_{\mathbf{f}}^{(\nu_0)}(t_l, \eta_k)) - \int_{R_l} g_\alpha(\eta - O_{\mathbf{f}}^{(\nu_0)}(t_l, \eta_k)) d\eta \right| \leq \frac{\Xi C_\alpha^3}{\sqrt{\pi} \Delta_r^3 d}$$

since the integrand is smooth and over R_l there are $\lfloor \frac{2\Delta_r d}{\Xi} \rfloor$ uniform discrete points.

Take the reassignment control in Corollary A.4 that

$$\max_l \max_{\substack{\eta \in (0, \Xi) \\ |V_{\mathbf{f}}^{(h)}(t_l, \eta)| > \tau}} |O_{\mathbf{f}}^{(\nu_0)}(t_l, \eta_k) - \phi'(t_l)| \leq \frac{E'_f + \Xi E_f}{\nu_0}.$$

By assumption, $\frac{E'_f + \Xi E_f}{\nu_0} \leq 1/2$, so we obtain

$$\left| \int_{R_l} g_\alpha(\eta - O_{\mathbf{f}}^{(\nu_0)}(t_l, \eta_k)) d\eta - 1 \right| \leq 2 \operatorname{erfc}(C_\alpha),$$

where we simply bound $\frac{E'_f + \Xi E_f}{\nu_0} < C_\alpha$ when ε is sufficiently small. As a result, when $\eta_k \in Q_l$, we have that

$$(47) \quad E_{g,l,k} := \frac{\Xi}{d} \sum_{\eta_j \in R_l} g_\alpha(\eta_j - O_{\mathbf{f}}^{(\nu_0)}(t_l, \eta_k)) - 1$$

satisfies

$$(48) \quad E_g := \max_l \max_{k \in Q_l} |E_{g,l,k}| \leq 2 \operatorname{erfc}(C_\alpha) + \frac{\Xi C_\alpha^3}{\sqrt{\pi} \Delta_r^3 d}.$$

When $\eta_k \notin Q_l$, we have $O_{\mathbf{f}}^{(\nu_0)}(t_l, \eta_k) = -\infty$, and hence $g_\alpha(\eta_j - O_{\mathbf{f}}^{(\nu_0)}(t_l, \eta_k)) = 0$, in which case we have

$$\frac{\Xi}{d} \sum_{\eta_j \in R_l} g_\alpha(\eta_j - O_{\mathbf{f}}^{(\nu_0)}(t_l, \eta_k)) = 0.$$

□

Lemma A.5. Grant the setup in Lemma A.4. Consider $\{Y_i\}_{i=1}^n$ follows model (11), where $f_i = f(t_i)$, f satisfies the AHM with $\varepsilon > 0$ and Assumption (2.1) fulfilled, $t_i = i/\sqrt{n}$, $\{\varepsilon_i\}_{i=1}^n$ satisfies the NSN model and Assumption 2.2, with the condition $A > \sqrt{\chi} + 1$ fulfilled, and $\sigma = \sigma(n) = n^{1/4 - \gamma'}$, where $\gamma' \in (0, 1/4]$ is a small constant. Set

$$\nu := \nu_0 + \zeta_n,$$

where ν_0 is defined in (45) and $\zeta_n \asymp n^{-\gamma'} \sqrt{\log n}$ is specified in (50). Then, when n is sufficiently large, with probability greater than $1 - n^{-2}$, we have

$$(49) \quad e_{g,l,k} := \frac{\Xi}{d} \sum_{\eta_j \in R_l} g_\alpha(\eta_j - O_Y^{(\nu/2)}(t_l, \eta_k)) - 1,$$

satisfying

$$e_g := \max_l \max_{\eta_k \in Q_l} |e_{g,l,k}| \leq E_g + \frac{108(1 + E_g)\Xi^2 C_\alpha^2}{\nu \Delta_r^2} \zeta_n,$$

where Q_l and R_l are defined in (44) and E_g is defined in (46). When $\eta_k \notin Q_l$, we have

$$\left| \frac{\Xi}{d} \sum_{\eta_j \in R_l} g_\alpha(\eta_j - O_Y^{(\nu/2)}(t_l, \eta_k)) - 1 \right| \leq e_g$$

when $|V_{\mathbf{f}}^{(h)}(t_l, \eta_k)| \geq \nu/2 + \zeta_n$ and

$$\begin{aligned} & \left| \frac{\Xi}{d} \sum_{\eta_j \in R_l} g_\alpha(\eta_j - O_Y^{(\nu/2)}(t_l, \eta_k)) \right| \\ & \leq \begin{cases} 0 & \text{when } |V_{\mathbf{f}}^{(h)}(t_l, \eta_k)| < \nu/2 - \zeta_n \\ \frac{2C_\alpha}{\pi} & \text{when } \nu/2 - \zeta_n \leq |V_{\mathbf{f}}^{(h)}(t_l, \eta_k)| < \nu/2 + \zeta_n. \end{cases} \end{aligned}$$

Remark. In general, note that the noise magnitude is controlled by $\sigma\zeta_n$, which assumed to decay to 0 when $n \rightarrow \infty$. Thus, the impact of noise is asymptotically negligible. Particularly, the trivial bound over the region of $\nu/2 - \zeta_n \leq |V_{\mathbf{f}}^{(h)}(t_l, \eta_k)| < \nu/2 + \zeta_n$ does not contribute significantly in our upcoming analysis since the measure of this region decays to 0 when $n \rightarrow \infty$.

When the data is noise-free, we have $e_g = E_g$, since ζ_n in the last term in e_g arises solely from controlling the noise magnitude. When $\eta_k \notin Q_l$, the bound $\left| \frac{\Xi}{d} \sum_{\eta_j \in R_l} g_\alpha(\eta_j - O_Y^{(\nu/2)}(t_l, \eta_k)) - 1 \right| \leq E_g$ holds when $|V_{\mathbf{f}}^{(h)}(t_l, \eta_k)| \geq \nu_0/2$. Therefore, when $\epsilon = 0$, we recover Lemma A.4 with the truncation threshold set to $\nu_0/2$.

Proof. We start with some observations. By the linearity of STFT and Lemma A.2, we know that with probability greater than $1 - n^{-3}$, $\max_l |\mathbf{V}_l|_\infty \leq C' \sqrt{\log d}$, and hence

$$\begin{aligned} (50) \quad & \max_{l,k} \max\{|V_{\sigma\epsilon}^{(\mathbf{h})}(t_l, \eta_k)|, |V_{\sigma\epsilon}^{(\mathbf{Dh})}(t_l, \eta_k)|\} \\ & \leq C' \sigma \sqrt{\log d} [\beta \sqrt{n}]^{-1/2} =: \zeta_n \asymp n^{-\gamma'} \sqrt{\log n}, \end{aligned}$$

where $C' > 0$, with probability higher than $1 - n^{-3}$. Denote the event subspace that (50) holds as Ω . On the other hand, by Corollary A.4, we know $\min_l \min_{\eta \in Q_l} |V_{\mathbf{f}}^{(h)}(t_l, \eta)| \geq \nu_0$. Clearly, since $\nu \geq \zeta_n$, when conditional on the event Ω , we have

$$\max_{l,k} |V_{\sigma\epsilon}^{(\mathbf{h})}(t_l, \eta_k)| \leq \nu,$$

and hence for any $\eta_k \in Q_l$, $|V_Y^{(\mathbf{h})}(t_l, \eta_k)| > ||V_{\mathbf{f}}^{(\mathbf{h})}(t_l, \eta_k)| - |V_{\sigma\epsilon}^{(\mathbf{h})}(t_l, \eta_k)|| \geq \nu/2$ holds since $\zeta_n \rightarrow 0$, and hence

$$(51) \quad \min_l \min_{k \in Q_l} |V_Y^{(\mathbf{h})}(t_l, \eta_k)| > \nu/2.$$

With the above preparation, we consider two cases: when $\eta_k \in Q_l$ and when $\eta_k \notin Q_l$. For the first case when $\eta_k \in Q_l$, since

$$\begin{aligned} (52) \quad & \frac{\Xi}{d} \sum_{\eta_j \in R_l} g_\alpha(\eta_j - O_Y^{(\nu/2)}(t_l, \eta_k)) = \frac{\Xi}{d} \sum_{\eta_j \in R_l} g_\alpha(\eta_j - O_{\mathbf{f}}^{(\nu_0)}(t_l, \eta_k)) \\ & + \frac{\Xi}{d} \sum_{\eta_j \in R_l} \left[g_\alpha(\eta_j - O_Y^{(\nu/2)}(t_l, \eta_k)) - g_\alpha(\eta_j - O_{\mathbf{f}}^{(\nu_0)}(t_l, \eta_k)) \right] \end{aligned}$$

and we have controlled $\frac{\Xi}{d} \sum_{\eta_j \in R_l} g_\alpha(\eta_j - O_{\mathbf{f}}^{(\nu_0)}(t_l, \eta_k))$ in Lemma A.4, the result is obtained by controlling the second term (52) caused by the NSN. Rewrite (52) as

$$\begin{aligned} & \frac{\Xi}{d} \sum_{\eta_j \in R_l} \left[g_\alpha(\eta_j - O_Y^{(\nu/2)}(t_l, \eta_k)) - g_\alpha(\eta_j - O_f^{(\nu_0)}(t_l, \eta_k)) \right] \\ &= \frac{\Xi}{d} \sum_{\eta_j \in R_l} \frac{1}{\sqrt{\pi\alpha}} e^{-\frac{1}{\alpha}|\eta_j - O_{\mathbf{f}}^{(\nu_0)}(t_l, \eta_k)|^2} \left(e^{-\frac{1}{\alpha}(|\eta_j - O_Y^{(\nu/2)}(t_l, \eta_k)|^2 - |\eta_j - O_f^{(\nu_0)}(t_l, \eta_k)|^2)} - 1 \right) \end{aligned}$$

For any $l = 1, \dots, n$, by (38) and (50), we have

$$\begin{aligned} & |O_Y^{(\nu/2)}(t_l, \eta_k) - O_{\mathbf{f}}^{(\nu_0)}(t_l, \eta_k)| \\ &= \left| \frac{V_{\sigma\varepsilon}^{(\mathbf{h}')} (t_l, \eta_k)}{V_Y^{(\mathbf{h})} (t_l, \eta_k)} - \frac{V_{\sigma\varepsilon}^{(\mathbf{h})} (t_l, \eta_k)}{V_Y^{(\mathbf{h})} (t_l, \eta_k)} O_{\mathbf{f}}^{(\nu_0)}(t_l, \eta_k) \right| \leq \frac{3\Xi}{\nu} \zeta_n \end{aligned}$$

when conditional on the event Ω , where we use the trivial bound $|O_{\mathbf{f}}^{(\nu_0)}(t_l, \eta_k)| + 1 \leq 1.5\Xi$ when ε is sufficiently small and (51). Therefore, since $\max_l \max_{k \in Q_l} |O_{\mathbf{f}}^{(\nu_0)}(t_l, \eta_k) + \eta_k| \leq 2\phi'(t_l)$ when ε is sufficiently small, we have $\max_l \max_{k \in Q_l} |O_Y^{(\nu/2)}(t_l, \eta_k) + \eta_k| \leq 3\phi'(t_l)$ when n is sufficiently large. On the other hand, since $\eta_j \in R_l$, we have $|O_{\mathbf{f}}^{(\nu_0)}(t_l, \eta_k) - \eta_j| \leq |O_{\mathbf{f}}^{(\nu_0)}(t_l, \eta_k) + \eta_k| + |\eta_k + \eta_j| \leq 4\phi'(t_l)$ and hence $|O_Y^{(\nu/2)}(t_l, \eta_k) - \eta_j| \leq 5\phi'(t_l)$. Therefore,

$$\begin{aligned} & \max_l \max_{k \in Q_l} \left| |\eta_j - O_Y^{(\nu/2)}(t_l, \eta_k)|^2 - |\eta_j - O_{\mathbf{f}}^{(\nu_0)}(t_l, \eta_k)|^2 \right| \\ & \leq \left(|O_Y^{(\nu/2)}(t_l, \eta_k) - \eta_j| + |O_{\mathbf{f}}^{(\nu_0)}(t_l, \eta_k) - \eta_j| \right) \left| O_Y^{(\nu/2)}(t_l, \eta_k) - O_{\mathbf{f}}^{(\nu_0)}(t_l, \eta_k) \right| \\ & \leq \frac{27\Xi^2}{\nu} \zeta_n. \end{aligned}$$

By Taylor expansion, we conclude that

$$\max_l \max_{k \in Q_l} \left| e^{-\frac{1}{\alpha}(|\eta_j - O_Y^{(\nu/2)}(t_l, \eta_k)|^2 - |\eta_j - O_{\mathbf{f}}^{(\nu_0)}(t_l, \eta_k)|^2)} - 1 \right| \leq \frac{108\Xi^2 C_\alpha^2}{\nu \Delta_r^2} \zeta_n.$$

Hence, with (47), we conclude the desired bound

$$\begin{aligned} & \max_l \max_{k \in Q_l} \left| \frac{\Xi}{d} \sum_{\eta_j \in R_l} \left(g_\alpha(\eta_j - O_Y^{(\nu/2)}(t_l, \eta_k)) - g_\alpha(\eta_j - O_{\mathbf{f}}^{(\nu_0)}(t_l, \eta_k)) \right) \right| \\ & \leq \left(\max_l \max_{k \in Q_l} \frac{\Xi}{d} \sum_{\eta_j \in R_l} \frac{1}{\sqrt{\pi\alpha}} e^{-\frac{1}{\alpha}|\eta_j - O_{\mathbf{f}}^{(\nu_0)}(t_l, \eta_k)|^2} \right) \\ & \quad \times \max_l \max_{k \in Q_l} \left| e^{-\frac{1}{\alpha}(|\eta_j - O_Y^{(\nu/2)}(t_l, \eta_k)|^2 - |\eta_j - O_{\mathbf{f}}^{(\nu_0)}(t_l, \eta_k)|^2)} - 1 \right| \\ & \leq \frac{108(1 + E_g)\Xi^2 C_\alpha^2}{\nu \Delta_r^2} \zeta_n. \end{aligned}$$

For the second case when $\eta_k \notin Q_l$, note that we get $O_{\mathbf{f}}^{(\nu_0)}(t_l, \eta_k) = -\infty$ and hence $g_\alpha(\eta_j - O_{\mathbf{f}}^{(\nu_0)}(t_l, \eta_k)) = 0$. By Corollary A.4, this case can only happen when $\eta_k \notin B_l$. We discuss three subcases: $|V_{\mathbf{f}}^{(\mathbf{h})}(t_l, \eta_k)| < \nu/2 - \zeta_n$, $\nu/2 + \zeta_n \leq |V_{\mathbf{f}}^{(\mathbf{h})}(t_l, \eta_k)| < \nu_0$, and $\nu/2 - \zeta_n \leq |V_{\mathbf{f}}^{(\mathbf{h})}(t_l, \eta_k)| < \nu/2 + \zeta_n$. In the first subcase,

since we have $|V_\epsilon^{(h)}(t_l, \eta_k)| < \zeta_n$ when conditional on Ω , $|V_Y^{(h)}(t_l, \eta_k)| \geq \nu/2$ cannot happen, and hence (52) is reduced to 0. In the second subcase, again, since we have $|V_\epsilon^{(h)}(t_l, \eta_k)| < \zeta_n$ when conditional on Ω , $|V_Y^{(h)}(t_l, \eta_k)| \geq \nu/2$ always happen, and $O_Y^{(\nu/2)}(t_l, \eta_k) \neq -\infty$. We need to evaluate $O_Y^{(\nu/2)}(t_l, \eta_k)$. Since $|V_f^{(h)}(t_l, \eta_k)| \geq \nu/2 + \zeta_n$ and E_f is of order ϵ , by the same argument as that for (38), when n is sufficiently large,

$$\begin{aligned} |O_Y^{(\nu/2)}(t_l, \eta_k) - \phi'(t_l)| &\leq \frac{\epsilon \Xi_A \left(\frac{J_0^{(0)}}{2\pi} + 3\Xi J_1^{(0)} + 2\pi \Xi^2 J_2^{(0)} \right) + (1 + \Xi)\zeta_n}{\nu/2} \\ &\quad + \frac{\Xi_A(\epsilon + \Xi + \|\mathbf{h}'\|_\infty + \|\mathbf{h}''\|_\infty)\beta}{\sqrt{n}\nu/2} \end{aligned}$$

Then, by the same argument as that for (47), we obtain

$$\left| \frac{\Xi}{d} \sum_{\eta_j \in R_l} g_\alpha(\eta_j - O_Y^{(\nu/2)}(t_l, \eta_k)) - 1 \right| \leq 2\text{erfc}(C_\alpha) + \frac{2\Xi C_\alpha^3}{\sqrt{\pi}\epsilon^{1/3}d}$$

and hence the desired bound. The third subcase is in general uncertain. Therefore, we only consider a trivial bound that

$$\left| \frac{\Xi}{d} \sum_{\eta_j \in R_l} g_\alpha(\eta_j - O_Y^{(\nu/2)}(t_l, \eta_k)) \right| \leq \frac{\Xi}{d} \sum_{\eta_j \in R_l} \frac{1}{\sqrt{\pi\alpha}} = \frac{2C_\alpha}{\pi}.$$

□

With the above lemmas, we are ready to prove the robustness theorem of SST reconstruction formula.

Proof of Theorem 4.2. Rewrite the targeting reconstruction formula at time t_l as

$$\begin{aligned} \tilde{f}^{\mathbb{C}}(t_l) &:= \frac{1}{\mathbf{h}(0)} \frac{\Xi}{d} \sum_{\eta_j \in R_l} S_Y^{(\mathbf{h})}(t_l, \eta_j) \\ &= \frac{1}{\mathbf{h}(0)} \frac{\Xi}{d} \sum_{\eta_j \in R_l} \frac{\Xi}{d} \sum_{k=1}^d V_Y^{(\mathbf{h})}(t_l, \eta_k) g_\alpha(\eta_j - O_Y^{(\nu/2)}(t_l, \eta_k)) \\ &= \frac{1}{\mathbf{h}(0)} \frac{\Xi}{d} \sum_{k=1}^d V_Y^{(\mathbf{h})}(t_l, \eta_k) I\left(|V_f^{(\mathbf{h})}(t_l, \eta_k)| > \frac{\nu}{2} - \zeta_n\right) \left[\frac{\Xi}{d} \sum_{\eta_j \in R_l} g_\alpha(\eta_j - O_Y^{(\nu/2)}(t_l, \eta_k)) \right], \end{aligned}$$

where $I(|V_f^{(\mathbf{h})}(t_l, \eta_k)| > \frac{\nu}{2} - \zeta_n)$ in the last equality comes from Lemma A.5. By the control of $\frac{\Xi}{d} \sum_{\eta_j \in B_l} g_\alpha(\eta_j - O_Y^{(\nu/2)}(t_l, \eta_k))$ in Lemma A.5 and the lower bound of $|V_f^{(\mathbf{h})}(t_l, \eta_k)|$ in Lemma A.4, we obtain

$$\begin{aligned} \tilde{f}^{\mathbb{C}}(t_l) &= \frac{1}{\mathbf{h}(0)} \frac{\Xi}{d} \sum_{k \in B_l} V_Y^{(\mathbf{h})}(t_l, \eta_k) (1 + e_{g,l,k}) \\ &\quad + \frac{1}{\mathbf{h}(0)} \frac{\Xi}{d} \sum_{k \in Q_l \setminus B_l} V_Y^{(\mathbf{h})}(t_l, \eta_k) (1 + e_{g,l,k}) \\ (53) \quad &\quad + \frac{1}{\mathbf{h}(0)} \frac{\Xi}{d} \sum_{k \notin Q_l} V_Y^{(\mathbf{h})}(t_l, \eta_k) I\left(|V_f^{(\mathbf{h})}(t_l, \eta_k)| > \frac{\nu}{2} - \zeta_n\right) e'_{g,l,k}, \end{aligned}$$

where $e'_{g,l,k}$ satisfies

$$(54) \quad |e'_{g,l,k}| \leq \begin{cases} e_g & \text{when } |V_{\mathbf{f}}^{(\mathbf{h})}(t_l, \eta_k)| \geq \frac{\nu}{2} + \zeta_n \\ \frac{2C_\alpha}{\pi} & \text{when } \frac{\nu}{2} - \zeta_n \leq |V_{\mathbf{f}}^{(\mathbf{h})}(t_l, \eta_k)| < \frac{\nu}{2} + \zeta_n \end{cases}$$

To obtain the desired claim, we control the right hand side of (53) term by term. The first term to control is $\frac{1}{\mathfrak{h}(0)} \frac{\Xi}{d} \sum_{k \in B_l} V_Y^{(\mathbf{h})}(t_l, \eta_k)$. By the linearity of STFT, consider the bound

$$\left| \frac{\Xi}{d} \sum_{k \in B_l} \left(V_Y^{(\mathbf{h})}(t_l, \eta_k) - V_{\mathbf{f}}^{(\mathbf{h})}(t_l, \eta_k) \right) \right| \leq \frac{\Xi}{d} \sum_{k \in B_l} |V_{\mathbf{e}}^{(\mathbf{h})}(t_l, \eta_k)| \leq 2\Delta\zeta_n,$$

where we use the fact that $\max_{l,k} |V_{\mathbf{e}}^{(\mathbf{h})}(t_l, \eta_k)| \leq \zeta_n$ (50). Therefore, we have when n is sufficiently large,

$$(55) \quad \frac{1}{\mathfrak{h}(0)} \frac{\Xi}{d} \sum_{k \in B_l} V_Y^{(\mathbf{h})}(t_l, \eta_k) = \frac{1}{\mathfrak{h}(0)} \frac{\Xi}{d} \sum_{k \in B_l} V_{\mathbf{f}}^{(\mathbf{h})}(t_l, \eta_k) + e_l,$$

where $\max_l |e_l| \leq 2\Delta\zeta_n$. With (55), we obtain

$$\left| \frac{1}{\mathfrak{h}(0)} \frac{\Xi}{d} \sum_{k \in B_l} V_Y^{(\mathbf{h})}(t_l, \eta_k) e_{g,l,k} \right| \leq (\Xi_A + E_r + 2\Delta\zeta_n) e_g,$$

where we use the STFT-based reconstruction formula analysis in (39). Therefore, the first term of (53) is controlled by

$$(56) \quad \left| \frac{1}{\mathfrak{h}(0)} \frac{\Xi}{d} \sum_{k \in B_l} V_Y^{(\mathbf{h})}(t_l, \eta_k) (1 + e_{g,l,k}) - A(t_l) e^{i2\pi\phi(t_l)} \right| \leq (E_r + 2\Delta\zeta_n)(1 + e_g) + \Xi_A e_g.$$

Since $e'_{g,l,k}$ and $V_Y^{(\mathbf{h})}(t_l, \eta_k)$ are small in the second and third terms of (53), we control them by trivial bounds. To this end, we prepare some quantities. We also need to control the size of $Q_l \setminus B_l$. By the decay property of $\widehat{\mathbf{h}}$, $Q_l \setminus B_l \subset [\Delta, C_h \Delta]$, where $C_h > 1$ depends on the property of \mathbf{h} . Therefore, with (54), we obtain the control for the second term:

$$(57) \quad \begin{aligned} & \left| \frac{\Xi}{d} \sum_{k \in Q_l \setminus B_l} V_Y^{(\mathbf{h})}(t_l, \eta_k) (1 + e_{g,l,k}) \right| \\ & \leq \frac{\Xi(1 + e_g)}{d} \sum_{k \in Q_l \setminus B_l} (|V_{\mathbf{f}}^{(\mathbf{h})}(t_l, \eta_k)| + \zeta_n) \\ & \leq (1 + e_g)(C_h - 1)\Delta(\nu_0 + \zeta_n). \end{aligned}$$

For the third term, we also need to control the size of $|V_{\mathbf{f}}^{(\mathbf{h})}(t_l, \eta_k)| \geq \nu/2 + \zeta_n$ when $k \notin Q_l$. Again, by the decay property of \mathbf{h} , and the fact that $Q_l^c \subset B_l^c$, the size of the set $\{k \notin Q_l \mid |V_{\mathbf{f}}^{(\mathbf{h})}(t_l, \eta_k)| \geq \nu/2 + \zeta_n\}$ is bounded by $C'_h \Delta$ for some constant $C'_h > C_h$. Similarly, the size of the set $\{k \notin Q_l \mid \nu/2 - \zeta_n < |V_{\mathbf{f}}^{(\mathbf{h})}(t_l, \eta_k)| \leq \nu/2 + \zeta_n\}$ is bounded by $C''\zeta_n$ for some $C'' > 0$ due to the smoothness of $|V_{\mathbf{f}}^{(\mathbf{h})}(t_l, \eta)|$ as a

function of η , where C'' depends on Ξ_A , Ξ and \mathbf{h} . As a result, we have

$$\begin{aligned}
(58) \quad & \left| \frac{\Xi}{d} \sum_{k \notin Q_l} V_Y^{(\mathbf{h})}(t_l, \eta_k) e'_{g,l,k} \right| \\
& \leq \left| \frac{\Xi}{d} \sum_{\substack{k \notin Q_l \text{ s.t.} \\ |V_{\mathbf{f}}^{(\mathbf{h})}(t_l, \eta_k)| \geq \nu/2 + \zeta_n}} (|V_{\mathbf{f}}^{(\mathbf{h})}(t_l, \eta_k)| + \zeta_n) \right| e_g \\
& \quad + \left| \frac{\Xi}{d} \sum_{\substack{k \notin Q_l \text{ s.t.} \\ \nu/2 - \zeta_n < |V_{\mathbf{f}}^{(\mathbf{h})}(t_l, \eta_k)| \leq \nu/2 + \zeta_n}} (|V_{\mathbf{f}}^{(\mathbf{h})}(t_l, \eta_k)| + \zeta_n) \right| \frac{2C_\alpha}{\pi} \\
& \leq \nu_0 [C'_h \Delta e_g + C'' C_\alpha \zeta_n].
\end{aligned}$$

Putting (56), (57) and (58) together, we conclude that

$$(59) \quad e_{r,l} := \tilde{f}^{\mathbb{C}}(t_l) - A(t_l) e^{i2\pi\phi(t_l)},$$

satisfies

$$\begin{aligned}
e_r := \max_l |e_{r,l}| & \leq (E_r + 2\Delta\zeta_n)(1 + e_g) + \Xi_A e_g \\
& \quad + (1 + e_g)(C_h - 1)\Delta(\nu_0 + \zeta_n) + \nu_0 [C'_h \Delta e_g + C'' C_\alpha \zeta_n] \\
& \leq 2E_r + 2C_h \Delta \nu_0 + \Xi_A e_g + (4 + 2C_h + C'' C_\alpha \nu_0) \zeta_n,
\end{aligned}$$

where the last bound is an immediate simplification by taking $e_g < 1$ into account. We further simplify this complicated bound to gain some insights. Since $m \asymp n^{1/2}$, $d \asymp n^{1/3-\gamma}$ and $\zeta_n \asymp n^{-\gamma'}$, when n is sufficiently large and conditional on the event Ω , we simplify e_r by keeping how noise impact the final result by keeping terms involving ζ_n . Simplify each error terms with the following trivial bounds:

$$e_g \leq 3\text{erfc}(C_\alpha) + \frac{162\Xi^2 C_\alpha^2}{\nu_0 \Delta_r^2} \zeta_n,$$

where we use the trivial bound that $E_g \leq 3\text{erfc}(C_\alpha) \leq 1.5$ and

$$E_r \leq 2\Xi_A \frac{\varepsilon J(\Xi + 1)\Delta + \beta^{-1/2}\delta_2}{\mathbf{h}(0)},$$

where we use the trivial bound $E_f \leq \varepsilon J \Xi_A (\Xi + 1)$ with $J := 2\pi \max_{k=1,2,3} J_k^{(0)}$. We thus obtain the desired simplified bound

$$(60) \quad e_r \leq C_1 \Xi_A + C_2 \zeta_n,$$

where

$$C_1 = 3\text{erfc}(C_\alpha) + C_h \Delta \sqrt{\beta} \delta_1 + \frac{2(\varepsilon J(\Xi + 1)\Delta + \beta^{-1/2}\delta_2)}{\mathbf{h}(0)}$$

and

$$C_2 := 4 + 2C_h + C'' C_\alpha \Xi_a \sqrt{\beta} \delta_1 + \frac{162\Xi_A \Xi^2 C_\alpha^2}{\Xi_a \sqrt{\beta} \delta_1 \Delta_r^2}.$$

□

A.5. Proof of Theorem 5.1.

Proof. Recall the existence of a Gaussian random process $\hat{\epsilon}_i$ that shares the same covariance structure of ϵ_i shown in Theorem 3.2. Under the given assumptions, we can well approximate $\hat{\epsilon}_i$, where $i = 1, \dots, n$, by a Gaussian tvAR process of order $b \in \mathbb{N}$ [10, Theorem 2.11], denoted as $\epsilon_i^{(*)}$, where $i = 1, \dots, n$, so that $\epsilon_i^{(*)} = \hat{\epsilon}_i$ in law for $i = 1, \dots, b$. Since we can find a sufficiently rich probability space to host ϵ_i^* and $\hat{\epsilon}_i$, $\hat{\epsilon}_i - \epsilon_i^*$ is Gaussian with mean 0, and the error is controlled by

$$(61) \quad \epsilon_i^{(*)} - \hat{\epsilon}_i = O_{\ell^2}(\log(b)^\tau b^{-(\tau-2)} + b^{2.5}n^{-1})$$

for $1 \leq i \leq n$. Since b is chosen to fulfill $\frac{b}{\log(b)} \asymp n^{1/(\tau+1)}$ to balance errors between the truncation and smooth approximation, the error becomes $O_{\ell^2}(n^{-\gamma})$, where $\gamma = \frac{\tau-2}{\tau+1} \in (0, 1]$; that is, we have

$$(62) \quad \max_{i=1, \dots, n} \|\epsilon_i^{(*)} - \hat{\epsilon}_i\|_2 \leq Cn^{-\gamma}$$

for some constant $C > 0$. Hence, if we denote the complex random vector associated with the discretized STFT of $\epsilon^{(*)} - \hat{\epsilon}$ by

$$\begin{aligned} E_1 := & [\Re V_{\epsilon^{(*)}-\hat{\epsilon}}^{(\mathbf{h})}(1, \eta_1), \Re V_{\epsilon^{(*)}-\hat{\epsilon}}^{(\mathbf{h}')} (1, \eta_1), \dots, \Re V_{\epsilon^{(*)}-\hat{\epsilon}}^{(\mathbf{h})}(n, \eta_1), \Re V_{\epsilon^{(*)}-\hat{\epsilon}}^{(\mathbf{h}')} (n, \eta_1), \\ & \Im V_{\epsilon^{(*)}-\hat{\epsilon}}^{(\mathbf{h})}(1, \eta_1), \Im V_{\epsilon^{(*)}-\hat{\epsilon}}^{(\mathbf{h}')} (1, \eta_1), \dots, \Im V_{\epsilon^{(*)}-\hat{\epsilon}}^{(\mathbf{h})}(n, \eta_1), \Im V_{\epsilon^{(*)}-\hat{\epsilon}}^{(\mathbf{h}')} (n, \eta_1), \\ & \Re V_{\epsilon^{(*)}-\hat{\epsilon}}^{(\mathbf{h})}(1, \eta_2), \Re V_{\epsilon^{(*)}-\hat{\epsilon}}^{(\mathbf{h}')} (1, \eta_2), \dots, \Re V_{\epsilon^{(*)}-\hat{\epsilon}}^{(\mathbf{h})}(n, \eta_2), \Re V_{\epsilon^{(*)}-\hat{\epsilon}}^{(\mathbf{h}')} (n, \eta_2), \\ & \dots \\ & \Im V_{\epsilon^{(*)}-\hat{\epsilon}}^{(\mathbf{h})}(1, \eta_d), \Im V_{\epsilon^{(*)}-\hat{\epsilon}}^{(\mathbf{h}')} (1, \eta_d), \dots, \Im V_{\epsilon^{(*)}-\hat{\epsilon}}^{(\mathbf{h})}(n, \eta_d), \Im V_{\epsilon^{(*)}-\hat{\epsilon}}^{(\mathbf{h}')} (n, \eta_d)]^\top \in \mathbb{R}^{4nd}, \end{aligned}$$

where $d \geq 1$ is the number of frequencies we have interest, we know E_1 is a Gaussian vector. Clearly, $\mathbb{E}E_1 = 0$. By (62), we claim that the entrywise standard deviation is controlled by

$$\beta_i := (\mathbb{E}|E_1(i)|^2)^{1/2} \leq C'n^{-\gamma},$$

where $C' > 0$ is a constant, for any $i = 1, \dots, 4nd$. Indeed, by taking $i = 1$ as an example, we have

$$\begin{aligned} \|E_1(1)\|_2 & \leq \frac{1}{n^{1/4}} \sum_{j=1-\lceil\beta\sqrt{n}\rceil}^{1+\lceil\beta\sqrt{n}\rceil} \left\| (\epsilon_j^{(*)} - \hat{\epsilon}_j) \mathbf{h}(j-1) \cos(2\pi\eta_1(j-1)) \right\|_2 \\ & \leq \frac{1}{n^{1/4}} \sum_{j=1-\lceil\beta\sqrt{n}\rceil}^{1+\lceil\beta\sqrt{n}\rceil} \left\| \epsilon_j^{(*)} - \hat{\epsilon}_j \right\|_2 \frac{1}{n^{1/4}} \mathbf{h} \left(-\beta + \frac{j-1}{\sqrt{n}} \right) \\ & \leq \max_{i=1, \dots, n} \left\| \epsilon_j^{(*)} - \hat{\epsilon}_j \right\|_2 \sum_{j=1-\lceil\beta\sqrt{n}\rceil}^{1+\lceil\beta\sqrt{n}\rceil} \frac{1}{\sqrt{n}} \mathbf{h} \left(-\beta + \frac{j-1}{\sqrt{n}} \right) \\ & \leq C'n^{-\gamma}, \end{aligned}$$

where $C' \leq 2\hat{h}(0)C$ by a Riemann sum approximation. Other entries are controlled by the same way, while noting that the Riemann sum approximation of $\hat{\mathbf{h}}'(0)$ decays

to 0 at the rate $n^{-1/2}$. A uniform bound of E_1 using the Gaussian tail bound is

$$\mathbb{P} \left\{ \max_{i=1, \dots, 4nd} |E_1(i)| > t \right\} \leq \sum_{i=1}^{4nd} \mathbb{P} \{|E_1(i)| > t\} \leq \sum_{i=1}^{4nd} e^{-\frac{t^2}{2\sigma_i^2}} \leq 4nde^{-\frac{t^2 n^{2\gamma}}{2C'^2}}.$$

Thus, for any large constant $D > 1$, we have

$$\mathbb{P} \left\{ \max_{i=1, \dots, 4nd} |E_1(i)| > Dn^{-\gamma} \sqrt{\log(n)} \right\} \leq n^{-2}$$

when n is sufficiently large. Denote \tilde{V}_i and \hat{V}_i to be the discretized STFT coefficients at time t associated with $\{\epsilon_i^*\}$ and $\{\hat{\epsilon}_i\}$ respectively; that is,

$$\begin{aligned} \tilde{V}_i &:= [V_{\epsilon^*}^{(\mathbf{h})}(t_i, \eta_1), \dots, V_{\epsilon^*}^{(\mathbf{h})}(t_i, \eta_d), V_{\epsilon^*}^{(\mathbf{h}')} (t_i, \eta_1), \dots, V_{\epsilon^*}^{(\mathbf{h}')} (t_i, \eta_d)]^\top \in \mathbb{C}^{2d}, \\ \hat{V}_i &:= [V_{\hat{\epsilon}}^{(\mathbf{h})}(t_i, \eta_1), \dots, V_{\hat{\epsilon}}^{(\mathbf{h})}(t_i, \eta_d), V_{\hat{\epsilon}}^{(\mathbf{h}')} (t_i, \eta_1), \dots, V_{\hat{\epsilon}}^{(\mathbf{h}')} (t_i, \eta_d)]^\top \in \mathbb{C}^{2d}, \end{aligned}$$

which are $2d$ -dim complex Gaussian random vectors. The above calculation suggests that with probability higher than $1 - O(n^{-2})$, we have

$$\max_{i=1, \dots, n} |\hat{V}_i - \tilde{V}_i| \leq C\sqrt{dn}^{-\gamma} \sqrt{\log(n)}$$

for some constant $C > 0$.

Next, by Theorem 3.2, if we denote V_i to be the discretized STFT coefficients associated with $\{\epsilon_i\}$; that is,

$$V_i := [V_{\epsilon}^{(\mathbf{h})}(t_i, \eta_1), \dots, V_{\epsilon}^{(\mathbf{h})}(t_i, \eta_d), V_{\epsilon}^{(\mathbf{h}')} (t_i, \eta_1), \dots, V_{\epsilon}^{(\mathbf{h}')} (t_i, \eta_d)]^\top \in \mathbb{C}^{2d},$$

then, since $m = \lceil \beta\sqrt{n} \rceil$, we have

$$\mathbb{E} \left(\max_l |V_t - \hat{V}_t| \right) \leq C' \left(\frac{d^{\frac{3}{4} - \frac{1}{2s} - \frac{1}{p}}}{n^{\frac{1}{4} - \frac{1}{2p} - \frac{1}{2s} + \frac{1}{ps}}} \right)^{\frac{1}{1 - \frac{1}{s} - \frac{1}{p}}} \log(n)^2,$$

and hence by Chebychev's inequality, we obtain

$$\max_l |V_t - \hat{V}_t| = o_p \left(\left(\frac{d^{\frac{3}{4} - \frac{1}{2s} - \frac{1}{p}}}{n^{\frac{1}{4} - \frac{1}{2p} - \frac{1}{2s} + \frac{1}{ps}}} \right)^{\frac{1}{1 - \frac{1}{s} - \frac{1}{p}}} \log(n)^3 \right).$$

By the above calculation, we have the control between the STFT of the original time series and the bootstrapped Gaussian time series by tvAR by

$$\begin{aligned} \max_{t=1, \dots, n} |V_t - \tilde{V}_t| &\leq \max_{t=1, \dots, n} |V_t - \hat{V}_t| + \max_{t=1, \dots, n} |\hat{V}_t - \tilde{V}_t| \\ (63) \quad &= o_p \left(\sqrt{dn}^{-\gamma} \sqrt{\log(n)} + \left(\frac{d^{\frac{3}{4} - \frac{1}{2s} - \frac{1}{p}}}{n^{\frac{1}{4} - \frac{1}{2p} - \frac{1}{2s} + \frac{1}{ps}}} \right)^{\frac{1}{1 - \frac{1}{s} - \frac{1}{p}}} \log(n)^3 \right) \end{aligned}$$

since in general $\sqrt{dn}^{-\gamma} \sqrt{\log(n)}$ and $\left(\frac{d^{\frac{3}{4} - \frac{1}{2s} - \frac{1}{p}}}{n^{\frac{1}{4} - \frac{1}{2p} - \frac{1}{2s} + \frac{1}{ps}}} \right)^{\frac{1}{1 - \frac{1}{s} - \frac{1}{p}}} \log(n)^3$ are not comparable.

Recall that the SST of $\{\epsilon_i\}$ is defined as

$$S_{\epsilon}^{(\mathbf{h})}(t_i, \xi_l) := \frac{\Xi}{d} \sum_{k=1}^d V_{\epsilon}^{(\mathbf{h})}(t_i, \eta_k) g_{\alpha}(\xi_l - O_{\epsilon}^{(\nu)}(t_i, \eta_k)) \in \mathbb{C}$$

for $i = 1, \dots, n$ and $\xi_l > 0$, and $S_{\epsilon^{(*)}}^{(\mathbf{h})}(t_i, \xi_l)$ is defined similarly from $\{\epsilon_i^*\}$. Denote $\mathbf{V}_{\epsilon, i} := [V_{\epsilon}^{(\mathbf{h})}(t_i, \eta_1), \dots, V_{\epsilon}^{(\mathbf{h})}(t_i, \eta_d)]^\top \in \mathbb{C}^d$ (the first d entries of \mathbf{V}_i), and $\mathbf{V}_{\epsilon^*, i}$ is defined similarly from $\{\epsilon_i^{(*)}\}$. Also denote

$$\mathbf{g}_i := \left[g_\alpha(\xi_l - O_\epsilon^{(\nu)}(t_i, \eta_1)), \dots, g_\alpha(\xi_l - O_\epsilon^{(\nu)}(t_i, \eta_d)) \right]^\top \in \mathbb{R}^d$$

and $\tilde{\mathbf{g}}_i$ is the associated random vector defined with $\{\epsilon_i^{(*)}\}$. We have

$$\begin{aligned} & \left| S_\epsilon^{(\mathbf{h})}(t_i, \xi_l) - S_{\epsilon^{(*)}}^{(\mathbf{h})}(t_i, \xi_l) \right| \\ &= \left| \frac{1}{d} \sum_{k=1}^d \left[V_{\epsilon}^{(\mathbf{h})}(t_i, \eta_k) g_\alpha(\xi_l - O_\epsilon^{(\nu)}(t_i, \eta_k)) - V_{\epsilon^{(*)}}^{(\mathbf{h})}(t_i, \eta_k) g_\alpha(\xi_l - O_{\epsilon^{(*)}}^{(\nu)}(t_i, \eta_k)) \right] \right| \\ &= \frac{1}{d} |(\mathbf{V}_{\epsilon, i} - \mathbf{V}_{\epsilon^*, i}) \cdot \mathbf{g}_i + \mathbf{V}_{\epsilon^*, i} \cdot (\mathbf{g}_i - \tilde{\mathbf{g}}_i)| \\ &\leq \frac{|\mathbf{V}_{Y, i}|}{d} |\mathbf{g}_i - \tilde{\mathbf{g}}_i| + \frac{|\mathbf{g}_i|}{d} |\mathbf{V}_i - \tilde{\mathbf{V}}_i|. \end{aligned}$$

Note that $|\mathbf{g}_i| \leq \sqrt{d/\alpha}$. Thus, combined with (63), the second term on the right hand side is controlled by $o_p \left(n^{-\gamma} \sqrt{\log(n)} + \frac{d^{-\frac{1}{2} + (\frac{3}{4} - \frac{1}{2s} - \frac{1}{p}) / (1 - \frac{1}{s} - \frac{1}{p})} \log(n)^3}{n^{(\frac{1}{4} - \frac{1}{2p} - \frac{1}{2s} + \frac{1}{ps}) / (1 - \frac{1}{s} - \frac{1}{p})}} \right)$. Since $n^{1/4} \mathbf{V}_{Y, i}$ is a non-degenerate d -dim complex Gaussian random vector with order 1 entrywise variance, $|\mathbf{V}_{Y, i}|$ can be bounded by $C \sqrt{d \log(d)} n^{-1/4}$ for some constant $C > 0$ with probability greater than $1 - n^{-2}$. Also, we can trivially bound $|\mathbf{g}_i - \tilde{\mathbf{g}}_i|$ by $2\sqrt{d/\alpha}$. As a result, the first term on the right hand side is controlled by $o_p(dn^{-1/4} \sqrt{\log(d)})$. As a result, for ξ_l ,

$$\begin{aligned} & \max_{j=1, \dots, n} |S_\epsilon^{(\mathbf{h})}(t_i, \xi_l) - S_{\epsilon^{(*)}}^{(\mathbf{h})}(t_i, \xi_l)| \\ &= o_p \left((n^{-\gamma} + dn^{-1/4}) \sqrt{\log(d)} + \frac{d^{-\frac{1}{2} + (\frac{3}{4} - \frac{1}{2s} - \frac{1}{p}) / (1 - \frac{1}{s} - \frac{1}{p})} \log(n)^3}{n^{(\frac{1}{4} - \frac{1}{2p} - \frac{1}{2s} + \frac{1}{ps}) / (1 - \frac{1}{s} - \frac{1}{p})}} \right). \end{aligned}$$

By a direct union bound, since $\frac{\frac{1}{4} - \frac{1}{2p} - \frac{1}{2s} + \frac{1}{ps}}{\frac{1}{2}(1 - \frac{1}{s} - \frac{1}{p}) + (\frac{3}{4} - \frac{1}{2s} - \frac{1}{p})} > 1/8$ for any p, s , we conclude that for ξ_1, \dots, ξ_d , when

$$a = \min \left\{ \gamma, \frac{\frac{1}{4} - \frac{1}{2p} - \frac{1}{2s} + \frac{1}{ps}}{\frac{1}{2}(1 - \frac{1}{s} - \frac{1}{p}) + (\frac{3}{4} - \frac{1}{2s} - \frac{1}{p})} \right\} - \vartheta,$$

where ϑ is any small positive constant so that $a \geq 0$, we have

$$\begin{aligned} & \max_{l=1, \dots, d} \max_{i=1, \dots, n} |S_\epsilon^{(\mathbf{h})}(t_i, \xi_l) - S_{\epsilon^{(*)}}^{(\mathbf{h})}(t_i, \xi_l)| \\ &= o_p \left((dn^{-\gamma} + d^2 n^{-1/4}) \sqrt{\log(d)} + \frac{d^{\frac{1}{2} + (\frac{3}{4} - \frac{1}{2s} - \frac{1}{p}) / (1 - \frac{1}{s} - \frac{1}{p})} \log(n)^3}{n^{(\frac{1}{4} - \frac{1}{2p} - \frac{1}{2s} + \frac{1}{ps}) / (1 - \frac{1}{s} - \frac{1}{p})}} \right) = o_p(1). \end{aligned}$$

□

APPENDIX B. MORE NUMERICAL RESULTS

Figures 7 and 8 present QQ plots comparing the distributions of the STFT and SST coefficients under the true noise model and those obtained via bootstrapping, evaluated at various time-frequency pairs. In these plots, columns correspond to

time points and rows to frequency levels. We only show the real part and the imaginary part is similar. The results demonstrate that the bootstrap-based distributions closely approximate those from the true noise model, validating the effectiveness of the bootstrapping approach.

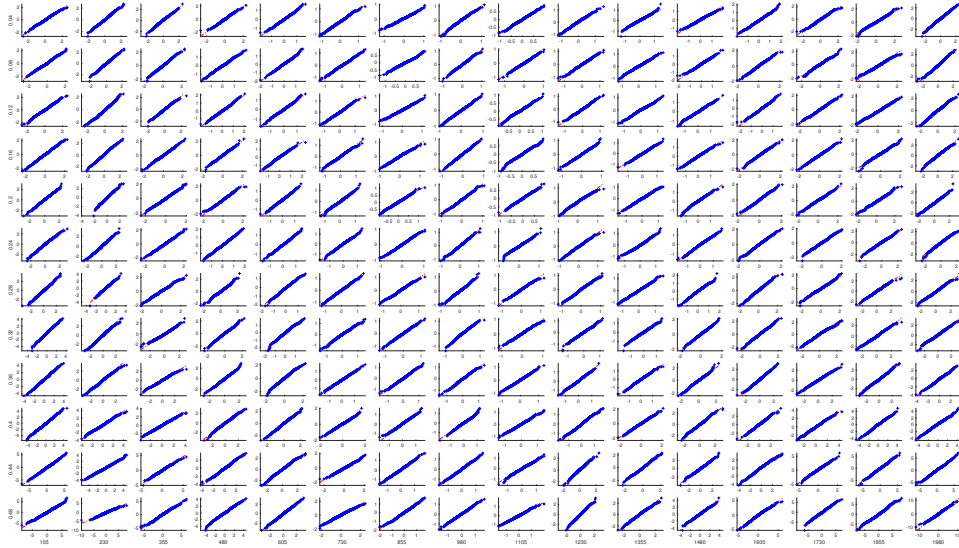


FIGURE 7. The QQ plot of the distribution of the real part of STFT of ϵ_i (null case) and its bootstrap.

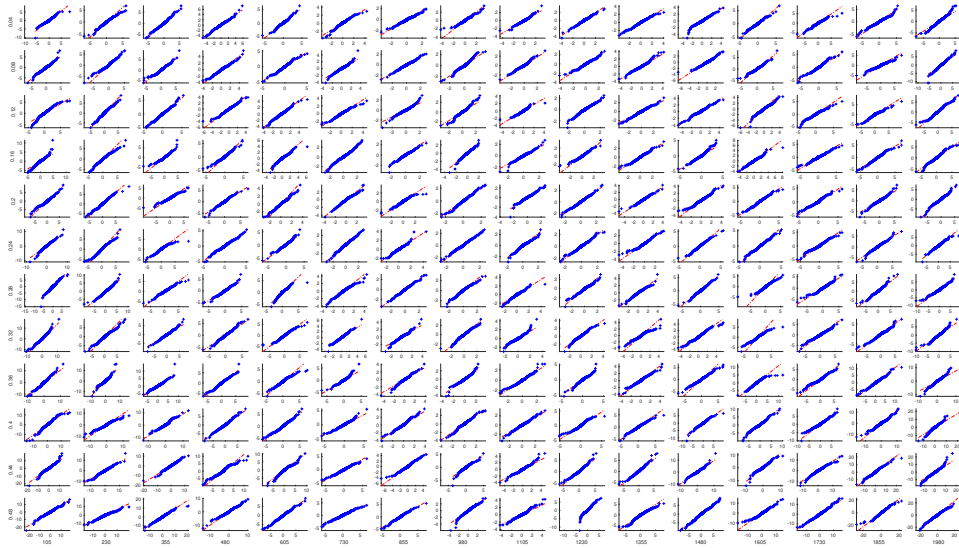


FIGURE 8. The QQ plot of the distribution of the real part of SST of ϵ_i (null case) and its bootstrap.

Under the non-null case, the QQ plots of the STFT and SST coefficient distributions comparing the true signal-plus-noise model with those obtained via bootstrapping are shown in Figures 9 and 10, respectively. Only the real parts are shown, as the imaginary parts exhibit similar behavior. The results demonstrate that, thanks to the robustness of the SST-based reconstruction algorithm, the bootstrap-based distributions closely approximate those from the true model. This supports the validity of combining SST-based reconstruction with the bootstrap approach.

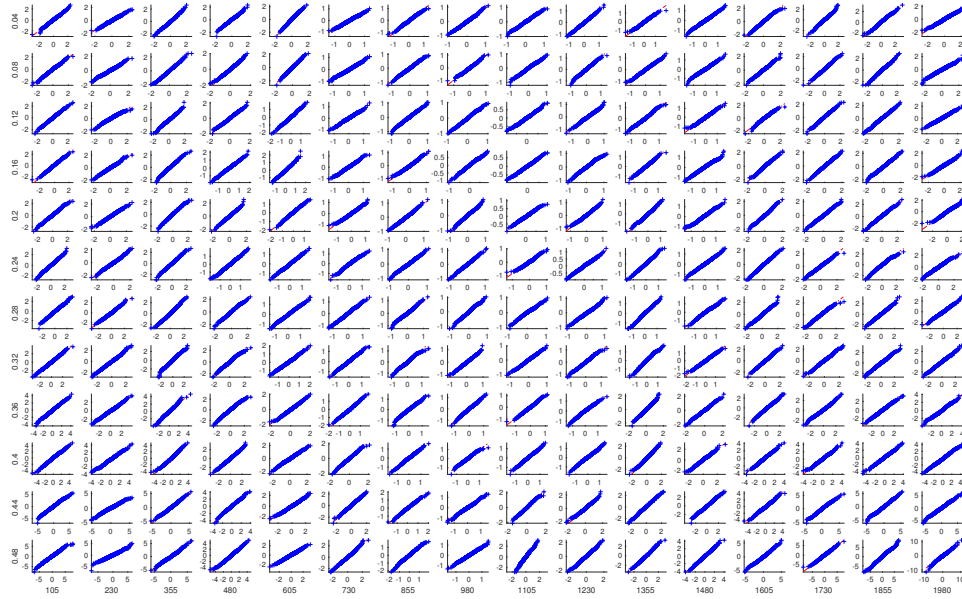


FIGURE 9. The QQ plot of the distribution of the real part of STFT of ϵ_i (nonnull case) and its bootstrap.

COURANT INSTITUTE OF MATHEMATICAL SCIENCES, NEW YORK UNIVERSITY, NEW YORK, 10012, USA

DEPARTMENT OF STATISTICS, UNIVERSITY OF TORONTO, TORONTO, ON, CANADA

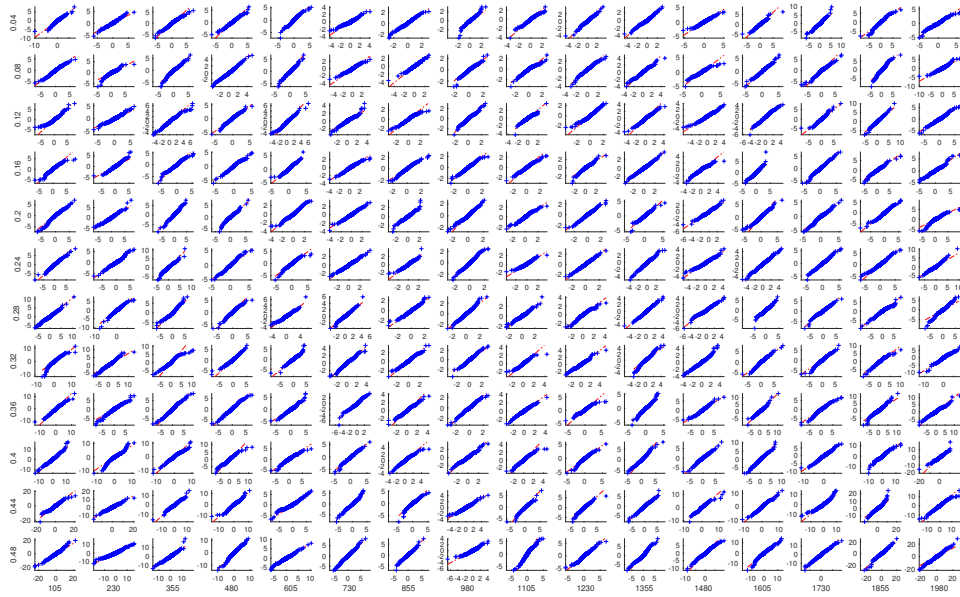


FIGURE 10. The QQ plot of the distribution of the real part of SST of ϵ_i (nonnull case) and its bootstrap.